AD-A177 884 DEVELOPMENT OF X-RAY LASER MEDIA: MEASUREMENT OF GAIN 1/1
AND DEVELOPMENT OF (U) ROCHESTER UNIV N Y LAB FOR
LASER ENERGETICS B YAAKOBI 30 SEP 85 AFOSR-TR-87-0037
UNCLASSIFIED AFOSR-81-0059 F/G 20/5 NL

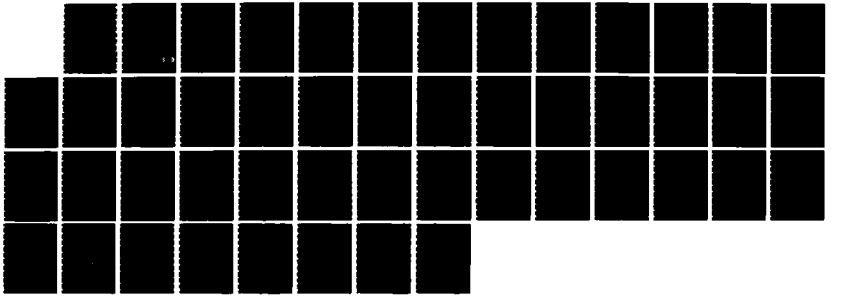

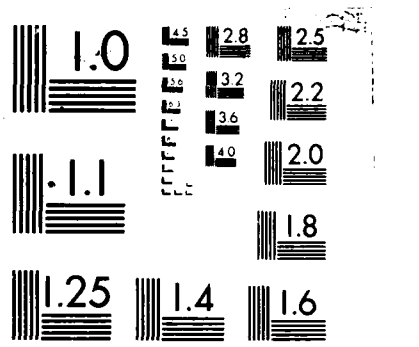

UNCLASSIFIED

SECURITY CLASSIFICATION OF THIS PAGE

(2)

EPORT DOCUMENTATION PAGE

AD-A177 004

1b. RESTRICTIVE MARKINGS

3. DISTRIBUTION/AVAILABILITY OF REPORT

Approved for public release, distribution unlimited

2b. DECLASSIFICATION/DOWNGRADING SCHEDULE

4. PERFORMING ORGANIZATION REPORT NUMBER(S)

5. MONITORING ORGANIZATION REPORT NUMBER(S)

AFOSR-TR- 87-0037

6a. NAME OF PERFORMING ORGANIZATION: University of Rochester

6b. OFFICE SYMBOL (If applicable):

7a. NAME OF MONITORING ORGANIZATION: AFOSR/NP

6c. ADDRESS (City, State and ZIP Code):
Laboratory for Laser Energetics
250 East River Road
Rochester, NY 14623-1299

7b. ADDRESS (City, State and ZIP Code):
Bldg 410
Bolling AFB, D.C. 20332-6448

8a. NAME OF FUNDING/SPONSORING ORGANIZATION: AFOSR

8b. OFFICE SYMBOL (If applicable): NP

9. PROCUREMENT INSTRUMENT IDENTIFICATION NUMBER: AFOSR-81-0059

8c. ADDRESS (City, State and ZIP Code): SAME AS 7b.

10. SOURCE OF FUNDING NOS.

PROGRAM ELEMENT NO.	PROJECT NO.	TASK NO.	WORK UNIT NO.
61102F	2301	A8	

11. TITLE (Include Security Classification): "DEVELOPMENT OF X-RAY LASERS" MEASUREMENT OF GAIN AND DEVELOPMENT OF CAVITY RESONATORS FOR WAVELENGTHS NEAR 130 ANGSTROMS", (Unclassified)

12. PERSONAL AUTHOR(S): Dr. Yaakobi

13a. TYPE OF REPORT	13b. TIME COVERED	14. DATE OF REPORT (Yr., Mo., Day)	15. PAGE COUNT
FINAL	FROM 81/01/01 TO 85/09/30		46

16. SUPPLEMENTARY NOTATION

17 COSATI CODES		
FIELD	GROUP	SUB. GR.

18. SUBJECT TERMS (Continue on reverse if necessary and identify by block number): X-ray, Laser, Plasma

19. ABSTRACT (Continue on reverse if necessary and identify by block number)

Gain of about three per cm over a lasing length of 13.6 mm was measured on the 3-to-2 transition of hydrogen-like carbon (CVI) at 182-angstroms. Laser-imploded, thin, cylindrical shells were investigated in the search for more efficient targets, new techniques were developed to fabricate the cylindrical shell targets. The details of x-ray emission from target plasmas were fully characterized.

20. DISTRIBUTION/AVAILABILITY OF ABSTRACT

UNCLASSIFIED/UNLIMITED ☒ SAME AS RPT ☒ DTIC USERS ☐

21. ABSTRACT SECURITY CLASSIFICATION: UNCLASSIFIED

22a. NAME OF RESPONSIBLE INDIVIDUAL	22b TELEPHONE NUMBER (Include Area Code)	22c. OFFICE SYMBOL
ROBERT J. BARKER	(202)767-5011	NP

DD FORM 1473, 83 APR EDITION OF 1 JAN 73 IS OBSOLETE.

UNCLASSIFIED

SECURITY CLASSIFICATION OF THIS PAGE

Final Report to:

AFOSR-TR- 87-0037

Air Force Office of Scientific Research

Arlington, Virginia 22209

AFOSR GRANT 81-0059

Submitted by:	Laboratory for Laser Energetics College of Engineering and Applied Science University of Rochester 250 East River Road Rochester, New York 14623-1299
Title of Project:	Development of X-Ray Laser Media: Measurement of Gain and Development of Cavity Resonators for Wavelengths Near 130 Angstroms.
Principal Investigator:	Barukh Yaakobi Senior Scientist Laboratory for Laser Energetics
Covering the Period:	January 1, 1984 - September 30, 1985

I. INTRODUCTION

Prior to the period covered by this report, work supported by this grant included the study of recombination-induced population inversion leading to short-wavelength lasing, and the design of optimal cavity mirrors for such lasing. The second of these two goals has been completed by 1984 and a detailed report has been submitted to AFOSR. A patent (No. 4,317,043) covering new developments in this area has been since granted to Alan Rosenbluth and James Forsyth of LLE, entitled:

"Normal Incidence X-Ray Reflectors and Resonant
Cavities for Supporting Laser Action Using the Same."

However, considerably more work was called for in the first area, namely better understanding the recombination mechanism and its utilization for generating population inversion on highly ionized atomic species and, eventually, demonstrating gain on short wavelength transitions. The present report shows that the goal of demonstrating gain has actually been achieved during the 1984-1985 period. Whereas previously we have only demonstrated population inversion between two excited levels (by measuring the intensity of transitions connecting these levels and the ground state), we have since demonstrated actual gain on the transition connected the two excited states which are inverted. The ability to achieve this was due, in large part, to the much greater laser energy which has become available to us in these experiments. This was achieved by moving from the single-beam GDL to the 24-beam, high-energy OMEGA laser system.

The proposal for the 1984 period recognized that to maximize the chances for significant inversion and hence gain, the target geometry has to be optimized and that the optimal configuration would not be the thick plane targets previously used. We have found, in fact, gain in thin-foil targets where the cooling due to expansion, leading to recombination inversion, is much more effective. Furthermore, we have studied extensively a more advanced geometry which we predict theoretically to be even more effective: that of laser-imploded thin cylindrical shells. We report here on theoretical and

experimental progress in this area. We have demonstrated for the first time the compression of cylindrical targets by a (multi-beam) laser. However, measurement gain with this type of targets awaits the availabilities or ..ill higher laser powers. We also report on the development work which went into the fabrication of these cylindrical targets. Considerable effort went into the design of cylindrical correcting plates which, when added to the focusing lenses on OMEGA produce short line focus; the alignment of a series of such line foci along one line produces a relatively abberation-free long line focus, appropriate for x-ray laser experiments.

II. PROPOSED PROGRAM FOR 1984

As a point of reference it would be useful to reproduce here the proposed 1984 program as it appeared in the submitted renewal request.

During the present, and proposed continuation period, we plan to concentrate much of our efforts on developing a basic understanding of processes in media which are strong candidates for use in the demonstration of soft x-ray laser action. We plant o elucidate the potential of the new target designs proposed in the previous section by a series of systematic experiments designed to test specific, individual features of these target designs.

The first experimental objective will be to determine the approximate thickness of target foils which using focused, frequency-tripled, Nd^{+3}:glass laser radiation, will produce a high concentration of fully stripped magnesium ions accelerating directly away from the rear target surface. We plan to begin these experiments during the current support period. There is considerable guidance in the choice of appropriate foil thickness range from layered target burn-through measurements in single beam irradiation geometry, and from hydrodynamic code calculations, which seem to agree well with single beam, point focus geometry. (Experimental test is still essential here, however, because we are interested in producing somewhat higher temperature conditions in the rear blowoff plasma

than is normally examined in such experiments.) Our examination of the frontside and backside blowoff characteristics will be made by spatially resolved, crystal, x-ray spectroscopy, a technique highly developed at LLE in this class of experiments.

At the end of this calendar year, substantially increased, frequency-tripled, laser intensity will be available for single beam experiments. We plan to use this opportunity to compare line focus and point focus burn-through conditions. This geometry has not previously been employed in burn-through studies and only crude guidance is available from spherical target experiments. (The estimate is that burn-through dimensions will be somewhat increased in line focus, compared to point focus geometry.)

In both line focus and point focus experiments, the effective burn-through distance will be determined by comparing the persistence of hydrogenic magnesium resonance line in the rear blowoff from very thin targets to that from successively thicker targets. A significant decrease in hydrogenic line emission would signify an overly thick foil.

When optimum foil thicknesses have been estimated in the two geometries, we will then add a heatsink structure to the rear side of the target. An identically aligned heatsink structure will probably be used in the front side of the foil in these experiments. This should permit easier alignment of both point and line focus laser beams with respect to the rearside heatsink, and should permit direct comparison of the performance of the two heatsinks in the expanding plasmas. Due to the number of possible heatsink geometries, it appears that optimizing the performance of the rearside heatsink may require most of the proposed continuation period. If this class of target designs shows early promise, we can begin to explore the addition of optical pumping via multiple beam configurations which will be in place by the beginning of the proposed continuation.

III. DESCRIPTION OF THE 1984-1985 RESULTS

In describing the results obtained during the period covered by this report, we rely on the relevant publications which are enclosed here as Appendices.

(A) Demonstration of Gain on the 182Å Line of CVI

Gain of about 3 cm^{-1} over a lasing length of 13.6 mm was measured on the $3 \rightarrow 2$ transition of hydrogen-like carbon (CVI), at 182Å. This experiment was done on OMEGA where up to eight line-focused beams were used to create the lasing medium. The target had a selenium layer over a Formvar layer, creating an additional cooling of the carbon plasma through the high x-ray radiation losses of the selenium component. This is an enhancement effect over the cooling due to expansion. Whereas in earlier work an enhancement of cooling was achieved through the plasma collision with unirradiated plates placed in front of the target, here the cooling is enhanced through radiation cooling. The results of this series of experiments are described in a paper entitled:

"Evidence for Gain on the CVI 182Å Transition in a
Radiation-Cooled Selenium/Formvar Plasma,"

which appeared in *Optics Communications*, Vol. 54, No. 5, p.289 (1985) and is reproduced here as Appendix I.

(B) Laser Implosion of Cylindrical Shell Targets

The search for more efficient target geometries (i.e., yielding a higher gain per unit length with a given laser power) led us to investigate the geometry of laser-imploded thin cylindrical shells. We found out by using our laser-fusion simulation codes that this geometry indeed holds a promise for significantly improved performance achievable with cylindrical shell targets. This is true for recombination-induced inversion but also, and more emphatically so, for inversion generated by electron collisions. The results show that cylinders imploded by a UV laser (such as the OMEGA laser) result in a higher-density

plasma, of wider lateral extent, and of a longer decay time than is achievable with exploding foils. The higher density leads to a higher gain per unit length (for the same temperature); the wider plasma reduces the refraction losses, thus permitting a longer length before refraction losses become prohibitive; finally the longer decay time increases the time-integrated intensity of the x-ray laser. The results of this theoretical analysis, as well as the actual demonstration on OMEGA of the compression of cylindrical shell targets were described in a paper entitled:

"Multibeam, Laser Imploded Cylindrical Plasmas,"

which appeared in the *Physical Review A*, Vol. 33, No. 2, p.1246 (Feb. 1986), and is reproduced here as Appendix II.

(C) Fabrication of Cylindrical Shell Targets

The fabrication of thin cylindrical shell targets required development of new techniques which were not available previously. Such techniques were mastered for the first time at LLE and promise to be crucial for x-ray laser experiments now being planned at various laboratories. These fabrication techniques are described in a paper entitled:

"Fabrication of Thin Cylindrical Targets for X-Ray Laser Experiments,"

which appeared in the *Journal of Vacuum Science and Technology*, Vol. A4, No. 3, p.1142 (May 1986), and is reproduced here as Appendix III.

(D) Characterization of X-Ray Emission

The general work of optimizing and characterizing the laser-target as an x-ray source continued during the period reviewed here. X-ray emission is relevant to x-ray laser studies for at least three reasons:

(i) as a source of cooling which impacts the inversion mechanism relying on recombination;

(ii) as a source of pumping in radiationally-pumped inversion schemes (which include both photoionization by continuum radiation and photoexcitation by line radiation);

(iii) as a signature of plasma behavior, thus of the attainment of conditions appropriate for inversion.

Additionally, laser-plasma x-ray emisison can be used (and has been used at LLE) for a variety of studies in biology and material studies. The work in this area was summarized in a paper entitled:

"Laser Generated X-Ray Source for Time-Resolved
Biological and Material Structure Studies,"

which appeared recently in a book published by Academic Press, entitled "Structural Biological Applications of X-Ray Absorption, Scattering, and Diffraction." A copy of this review paper is enclosed here as Appendix IV.

Appendix I

EVIDENCE FOR GAIN ON THE C VI 182 Å TRANSITION IN A RADIATION-COOLED SELENIUM/FORMVAR PLASMA

J.F. SEELY, C.M. BROWN, U. FELDMAN

E.O. Hulburt Center for Space Research, Naval Research Laboratory, Washington, DC 20375-5000, USA

M. RICHARDSON, B. YAAKOBI

Laboratory for Laser Energetics, University of Rochester, Rochester, NY 14623-1299, USA

and

W.E. BEHRING

Laboratory for Solar Physics and Astrophysics, Goddard Space Flight Center, Greenbelt, MD 20771, USA

Received 19 February 1985

Thin plastic foils coated with selenium have been irradiated using from 4 to 8 beams of the OMEGA laser in a line focus configuration. Spectra were recorded using a 3 meter spectrograph that viewed the plasma along the line focus. Based on a comparison of the intensities of the spectral lines from plasmas with lengths of 1.7, 3.4, 6.8, and 13.6 mm, the C VI $n = 3$ to 2 transition at 182 Å was anomalously intense in the spectra from the longer plasmas. Calculations indicate that the carbon plasma was cooled by radiation from the highly-charged selenium plasma in a time that was smaller than the expansion time of the plasma. These plasma conditions are favorable for the occurrence of population inversions between the $n = 2$ and 3 levels of C VI resulting from recombination and cascading from higher levels. The measured gain coefficient for the C VI 182 Å transition is 3 cm^{-1}, and this corresponds to a gain-length product of 4 in the longest plasma.

1. Introduction

Amplification on transitions in selenium (206.3 Å and 209.6 Å) and yttrium (155.0 Å and 157.1 Å) in a laser-produced plasma has recently been reported [1,2]. Thin foils of Formvar plastic coated with selenium or yttrium were irradiated by one or two beams of the Novette laser in a line focus configuration.

A related series of experiments has been performed using the OMEGA laser system at the University of Rochester. Using six frequency-tripled beams of the OMEGA laser, solid targets composed of the elements Cu, Zn, Ga, Ge, As, Se, Br, and Rb (atomic numbers $Z = 29$–35 and $Z = 37$) were spherically irradiated, and the spectra in the range 20 Å to 370 Å were recorded by a 3 meter grazing incidence spectrograph [3,4]. More recently, selenium/Formvar targets were irradiated using from 4 to 8 beams in a line focus configuration. The intensity of the C VI 128 Å transition increased anomalously with the length of the foil targets. As discussed below, calculations indicate that the radiation cooling time for the highly-charged selenium plasma was smaller than the expansion time of the selenium/carbon plasma. These plasma conditions favor the occurrence of inversions between the $n = 2$ and 3 levels of C VI resulting from rapid recombination and cascading from higher levels.

The conditions for gain to occur on C VI transitions in an expanding cylindrical plasma have been calculated by Pert [5]. Typical results are shown in fig. 1 for expansion from a carbon fiber 40 μm in diameter. The gain coefficient on the C VI $n = 3$ to 2 transition reaches a value of approximately 5 cm^{-1} in a time of 0.5 ns. Experiments have been performed in which

0 030-4018/85/$03.30

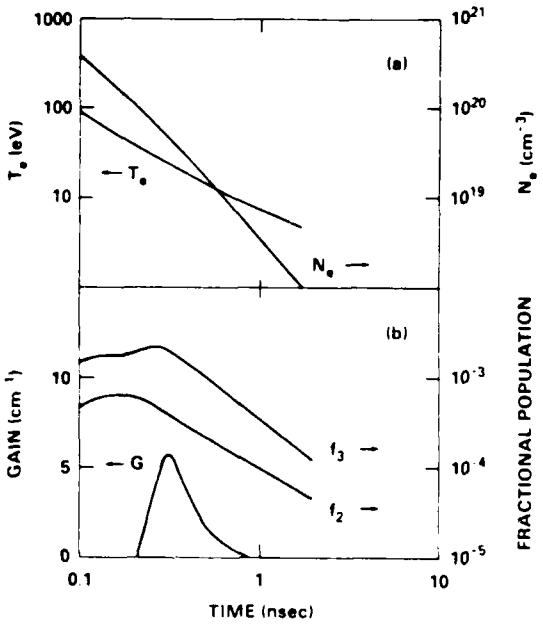

Fig. 1. The electron temperature and the electron density (a) and the C VI excited state populations and the gain on the $n = 2-3$ transition at 182 Å (b) for a carbon plasma expanding from a fiber 40 μm in diameter (from ref. [5]).

gain–length products (GL) up to 5 were measured in carbon [6]. Suckewer and Fishman [7] calculated the conditions for radiatively cooling a linear carbon plasma that is confined by a solenoidal magnetic field, and values of GL up to 6.5 have been measured by Suckewer and coworkers [8,9]. Matthews et al. [10] measured GL = 0.6 for the O VIII $n = 3$ to 2 transition in a plasma produced from an uncoated Formvar foil irradiated by the Novette laser.

Population inversions on transitions in hydrogenic ions with $Z = 6$ to 13 have been experimentally demonstrated using other cooling techniques. These include rapid expansion from laser-heated planar targets [11,12], the interaction of the expanding plasma with a baffle [13] and a background gas [14,15], and radiation from high-Z components in expanding laser-produced plasmas [16,17].

Plasma cooling by the emission of photons from the resonance level of an ion is rapid when the plasma temperature kT_e is comparable to the excitation energy ΔE of the level. When kT_e falls much below ΔE, the collisional population of the resonance level from the ground state is slow, and the emission from the resonance level decreases. In this case, the cooling of a laser-produced plasma is due primarily to adiabatic expansion. However, the plasma density also decreases during expansion, and this results in a low density of recombining ions. For an expanding plasma composed of ions with highly excited resonance levels, such as hydrogen-like and helium-like ions, it is difficult to achieve rapid cooling to a low temperature and also maintain a moderately high plasma density that is necessary for high gain on inverted transitions.

As first pointed out by Konokov and Koshelev [18], rapid radiative cooling over a wide range of temperature can be achieved in an expanding plasma if an abundance of ions in the configuration $1s^2\,2s^n\,2p^m$ is present. For these configurations, the resonance levels are not far above the ground state, and the condition $kT_e \approx \Delta E$ occurs over a wide range of temperature and down to low temperature. As the high-Z plasma cools and recombines, radiation cooling continues to occur over a series of lower ionization stages with resonance levels that are progressively closer to the ground state.

In related work [19], a thin film of carbon (vacuum grease dissolved in benzine) was deposited on a KCl crystal substrate. The thickness of the carbon film was varied in order to produce the highest ratio of the 3–4 and 2–4 transitions. The optimal film thickness of approximately 3000 Å resulted in an increase in the 3–4, 2–4 intensity ratio by a factor of 1.5.

2. Experimental results

The use of selenium/Formvar foil targets in our experiments was inspired by the recently successful Livermore work [1,2]. Our Formvar foil was 1000 Å thick, and a coating of selenium 750 Å thick was deposited on one side of the foil. The foil was supported by an aluminum holder. This holder obscured the plasma at distances greater than 200 μm from the foil on the Formvar side of the target. The plasma near the target on the selenium side was unobscured.

Frequency-tripled beams from the OMEGA laser system were focused onto the targets using cylindrical corrector lenses mounted inside the target chamber. The focal spot for each beam was approximately 100 μm wide and 1.7 mm long. The average energy in each

beam was typically 70 J, and approximately 30% of the energy was absorbed by the target. The pulse duration was 600 ps. Except as noted below, the laser beams were incident nearly perpendicular to the foil surface.

The plasmas 1.7 mm in length were produced by irradiating the foil targets using four laser beams, with two completely overlapping focal spots on each side of the target. The 3.4 mm plasmas were produced by four laser beams, with two offset laser beams from each side of the foil. The focal spots on each side of the target were contiguous. The 6.8 mm plasmas were produced by four offset beams, two from each side. The 13.6 mm plasmas were produced by eight offset beams, two from each quadrant. In this latter case, the foil was rotated so the beams were incident on the target at an angle of approximately 45° from the normal to the foil.

The spectra were recorded using a 3 meter grazing incidence spectrograph that has been described in ref. [20]. The spectrograph was fitted with a 1200 line/mm gold-coated Bausch and Lomb replica grating. A cylindrical beryllium mirror was positioned in front of the entrance slit and 1.3 m from the target. The linear image formed by the mirror was at a small angle (approximately 10°) to the entrance slit, and this resulted in a small amount of spatial resolution across the photographic plate. Kodak 101 plates were used, the entrance slit was 10 μm wide, and three exposures were integrated onto each plate.

Spectral lines were observed from 20 Å to 370 Å. Spectral lines from Se XXVII, Se XXVI, Se XXIV, and Se XXIII have been identified. These lines were identified by extrapolation and interpolation of measured wavelengths for the elements Cu, Zn, Ga, Ge, As, Br, and Rb [3,4] and from calculated wavelengths and intensities for Se [21,22]. The wavelengths were measured to an accuracy of better than 0.02 Å. Where comparisons can be made, the measured wavelengths agree quite well with the measurements of Kononov [23] for Se XXIV and with the recommendations of Edlén [24] for Se XXVI and Se XXVII. Spectral lines do not appear at 206.3 Å and 209.6 Å on any of the plates, although a third-order Se XXIV line does appear at 209.4 Å. We have identified no lines from neon-like Se XXV. Several lines from Al XI, O VI, C V, and C VI have been identified.

A comparison was made of the four sets of plates

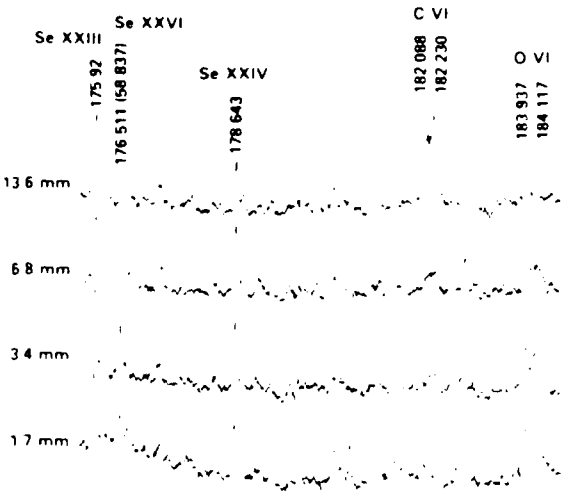

Fig. 2. The spectra in the wavelength range 175 Å to 185 Å for selenium Formvar plasmas of lengths 1.7, 3.4, 6.8 and 13.6 mm. The intensity of the C VI $n = 3$ to 2 feature at 182 Å increases anomalously with the length of the plasma. The total laser energy and the focused intensity on target for the four plasma lengths are the following: 1.7 mm (280 J, 1.4×10^{14} W/cm^2), 3.4 mm (280 J, 7×10^{13} W/cm^2), 6.8 mm (280 J, 7×10^{13} W/cm^2), and 13.6 mm (560 J, 7×10^{13} W/cm^2).

from plasmas with lengths 1.7, 3.4, 6.8 and 13.6 mm. Only the C VI 2–3 line showed a dramatic increase in intensity with plasma length (see fig. 2). Using the O VI 183.937 Å and 184.117 Å lines as references [25], the wavelengths of the C VI doublet were measured to be 182.10 Å and 182.22 Å. This agrees, to within the experimental uncertainty of 0.02 Å, with the calculated wavelengths 182.088 Å and 182.230 Å of the $2p\ ^2P_{1/2}-3d\ ^2D_{3/2}$ and $2p\ ^2P_{3/2}-3d\ ^2D_{5/2}$ transitions [26]. These two transitions have the largest gf values (1.392 and 2.505, respectively) of the seven C VI 2–3 components, where g is the statistical weight of the lower level and f is the absorption oscillator strength.

We note in fig. 2 that the relative intensities of the O VI, Se XXIII, Se XXIV, and Se XXVI lines remained approximately constant as the length of the plasma was varied. This implies that the plasma ionization balance and temperature were nearly the same for all four lengths. Based on the ionization stages of selenium that were produced, we estimate that the peak electron temperature in the selenium plasma was greater than 1000 eV.

The C V $1s2p\ ^3P_1-1s3d\ ^3D_2$ and $1s2p\ ^3P_2-1s3d\ ^3D_3$ transitions (248.661 Å and 248.738 Å) were identified on all four plates, and the intensities of these transitions did not vary appreciably with plasma length. The C V $1s2p\ ^3P-1s4d\ ^3D$ transitions were not identified. The C VI $n = 1-2$ (33.740 Å) and C V $1s^2\ ^1S_0-1s2p\ ^1P_1$ (40.2680 Å) transitions were identified, but they were very weak. These latter two transitions were absent in the second and higher orders.

The selenium spectral lines from the linear plasmas are much narrower than from point plasmas [3,4]. This is probably due to a reduction in the ion velocities parallel to the axis of the linear plasma [27]. The width of the C VI 182.230 Å transition is 80 mÅ. The instrumental width, resulting from the use of a 10 μm entrance slit, is 28 mÅ. Assuming gaussian profiles and removing the instrumental broadening, the resulting width of 75 mÅ corresponds to an axial expansion velocity of 1×10^7 cm/s. Assuming an electron temperature of 50 eV and an electron density of 10^{19} cm^{-3}, which are typical of recombining carbon plasmas, the contributions of thermal Doppler broadening and of Stark broadening [28] to the linewidth are small.

3. Discussion

Listed in table 1 are the relative intensities of the C VI 2–3 and 2–4 transitions for plasmas of length 6.8 mm and 13.6 mm. These relative intensities were measured using the calibration curve for Kodak 101 emulsion that was determined by the multiple-exposure technique. For the plasmas of length 1.7 mm and 3.4 mm, the C VI lines were too weak for reliable intensity measurements. When the plasma length was increased from 6.8 mm to 13.6 mm, the intensity of the 2–4 transition increased by 1.3, while the intensity of the 2–3 transition increased by 5.5. For these two plasma lengths, the incident laser energy per plasma length and the focused laser intensity were held constant at 41 J/mm and 7×10^{13} W/cm^2, respectively.

Table 1
Relative intensities of the C VI $n = 2$ to 3 (182 Å) and $n = 2$ to 4 (135 Å) transitions for selenium/Formvar plasmas.

Plasma length (mm)	Relative intensities 2–3	2–4
6.8	7.2	12.0
13.6	39.4	15.9

We apply the expression for the intensity of amplified spontaneous emission in an unsaturated gain medium,

$$I = i(e^{GL} - 1)/G \qquad (1)$$

to each of the two plasmas (6.8 mm and 13.6 mm in length). In eq. (1), i is the spontaneous emission per length, and I is the amplified emission. The gain per length G for the 2–3 transition is assumed to be the same in the two plasmas. Then we obtain

$$I_2/I_1 = (i_2/i_1)(e^{GL_2} - 1)/(e^{GL_1} - 1)\,, \qquad (2)$$

where the subscripts 1 and 2 refer to the 6.8 mm and 13.6 mm plasmas, respectively. The ratio of amplified emission I_2/I_1 is equal to 5.5.

Due to the shorter wavelength and the smaller spontaneous decay rate of the C VI 2–4 transition, the gain on this transition, if the levels are inverted at all, is expected to be more than an order of magnitude smaller than the gain on the 2–3 transition. We assume that the ratio of spontaneous emission per length i_2/i_1 for the 2–4 transition is the same as for the 2–3 transition [9]. Then i_2/i_1 in eq. (2) is equal to 0.7, and the calculated gain coefficient is $G = 3$ cm^{-1}. This corresponds to a gain–length product (GL) of 4 in the 13.6 mm plasma.

We believe that the population inversion between the C VI $n = 2$ and 3 levels results from recombination in the carbon, selenium plasma that has been rapidly cooled by radiation from the highly-charged selenium ions. More than 200 spectral lines appear on the plates between 20 Å and 370 Å. Many of these lines are from Se XXVII, Se XXVI, Se XXIV, and Se XXIII. All of these ions have low-energy resonance levels. The energy radiated in a line is given by $N_i f_2 A_{21} h\nu_{21}$, where N_i is the density of the ground state of the ion, f_2 is the fractional population of the excited level, and A_{21} is the spontaneous decay rate. For a typical [21] emission rate $f_2 A_{21}$ (per ion and per line) of 10^{10} photons s^{-1} and assuming a selenium ion density of 5×10^{19} cm^{-3}, it is estimated that the total emission rate from the selenium plasma is approximately 10^{34} eV s^{-1} cm^{-3}. Assuming an electron den-

sity of 10^{21} cm^{-3} and a temperature of 1000 eV, the thermal energy density ($N_e kT_e$) of the plasma is 10^{24} eV cm^{-3}. The cooling time is therefore approximately 100 ps. By comparison, the time for the selenium plasma to expand (at the ion sound velocity of 2×10^7 cm s) is approximately 500 ps.

The reabsorption of C VI Lyman-alpha photons, which populates the $n = 2$ level and tends to quench the $n = 2-3$ population inversion, is of concern in carbon plasmas that are produced from relatively thick solid targets [5]. For a carbon plasma 200 μm in size, the C VI 1–2 transition is optically thick for a C VI ground state population greater than 10^{17} cm^{-3}. In a pure carbon plasma, the plasma conditions of high electron density (for rapid recombination and large excited state populations) and low C VI density (for an optically thin C VI 1–2 transition) are difficult to achieve. In our selenium Formvar plasma, an abundance of electrons is supplied from the highly-ionized selenium, and for a given electron density, the C VI density is lower than in a pure carbon plasma.

The composition of Formvar (polyvinyl formal) is $C_{11}H_{18}O_5$. The O VIII $n = 2-3$ line at 102.43 Å was very weak on all four plates and showed no anomalous increase in intensity with plasma length. Since the relative abundance of oxygen in the target was a factor of 2.2 smaller than for carbon and since the gain coefficient scales as λ^3, the gain on the O VIII 2–3 transition is expected to be more than an order of magnitude smaller than the gain on the C VI 2–3 transition. For a gain of GL = 4 on the C VI 2–3 transition, we would not expect to observe an anomalous increase in the intensity of the O VIII 2–3 transition in our time-integrated data.

4. Conclusions and future work

We have presented evidence for gain on the C VI 2–3 transition at 182 Å in a selenium Formvar plasma. Based on the increase in the intensity of the C VI 2–3 transition with the length of the plasma, measured relative to the intensity of the C VI 2–4 transition, the gain coefficient for the C VI 2–3 transition is estimated to be 3 cm^{-1}. These results are based on one series of experiments, and we plan to extend these initial measurements by varying the target metal coating and foil materials and by producing longer plasmas using additional beams of the 24-beam OMEGA laser.

It is likely that the combination of selenium and carbon is not the optimal pair of elements. Considering the high critical electron density that results from the use of frequency-tripled (351 nm) laser radiation and the high electron temperature of the selenium plasma, gain in O VIII and F IX should be measurable if the abundance of these ions can be increased. Conversely, the high-Z component of the plasma could be changed from selenium to another metal such as Ga or Zn. The choice will be strongly influenced by the availability of thin plastic films (with high abundances of O and F) and of thin metal coatings.

An attractive feature of lasing on an allowed $\Delta n = 1$ transition is that the wavelength scales strongly with Z. The wavelengths of the $n = 2-3$ transitions in O VIII and F IX are 102.43 Å and 80.91 Å, respectively. At these shorter wavelengths, the opacity of the $n = 1-2$ transition is smaller, and this allows the use of a plasma with a larger transverse dimension and a higher hydrogenic ground-state population.

Acknowledgements

This work would not have been possible without the expert technical assistance of G. Gregory, W. Watson, and the OMEGA operations staff. We also acknowledge useful discussions with S. Suckewer.

The work performed at the Naval Research Laboratory was supported by the U.S. Department of Energy under Contract DE-AI08-84DP40092:26. Research and materials were partially developed at the National Laser Users Facility at the University of Rochester's Laboratory for Laser Energetics, with financial support from the U.S. Department of Energy under Contract DE-FC08-85DP40200.

References

[1] D.L. Matthews, P.L. Hagelstein, M.D. Rosen, M.J. Eckart, N.M. Ceglio, A.U. Hazi, H. Medecki, B.J. MacGowan, J.E. Trebes, B.L. Whitten, E.M. Campbell, C.W. Hatcher, A.M. Hawryluk, R.L. Kauffman, L.D. Pleasance, G. Rambach, J.H. Scofield, G. Stone and T.A. Weaver, Phys. Rev. Lett. 54 (1985) 110.

[2] M.D. Rosen, P.L. Hagelstein, D.L. Matthews, E.M. Campbell, A.U. Hazi, B.L. Whitten, B. MacGowan, R.E. Turner, R.W. Lee, G. Charatis, Gar. E. Busch, C.L. Shepard, P.D. Rockett and R.R. Johnson, Phys. Rev. Lett. 54 (1985) 106.
[3] W.E. Behring, J.F. Seely, Samuel Goldsmith, Leonard Cohen, M. Richardson and U. Feldman, J. Opt. Soc. Am. B, to be published.
[4] J.F. Seely, U. Feldman, W.E. Behring and M. Richardson, J. Opt. Soc. Am. B, to be published.
[5] G.J. Pert, J. Phys. B9 (1976) 3301.
[6] D. Jacoby, G.J. Pert, S.A. Ramsden, L.D. Shorrock and G.J. Tallents, Optics Comm. 37 (1981) 193.
[7] S. Suckewer and H. Fishman, J. Appl. Phys. 51 (1980) 1922.
[8] S. Suckewer, C.H. Skinner, D.R. Voorhees, H.M. Milchberg, C. Keane and A. Semet, IEEE J. Quantum Electr. QE19 (1983) 1855.
[9] S. Suckewer, C. Keane, H. Milchberg, C.H. Skinner and D. Voorhees, in: Laser techniques in the extreme ultraviolet, AIP Conf. Proc. No. 119, eds. S.E. Harris and T.B. Lucatorto (AIP, New York, 1984). See also Bull. Am. Phys. Soc. 29 (1984) 1211, and to be published.
[10] D.L. Matthews, E.M. Campbell, K. Estabrook, W. Hatcher, R.L. Kauffman, R.W. Lee and C.I. Wang, Appl. Phys. Lett. 45 (1984) 226.
[11] F.E. Irons and N.J. Peacock, J. Phys. B7 (1974) 1109.
[12] M.H. Key, C.L.S. Lewis and M.J. Lamb, Optics Comm. 28 (1979) 331.
[13] V.A. Bhagavatula and B. Yaakobi, Optics Comm. 24 (1978) 331.
[14] R.H. Dixon and R.C. Elton, Phys. Rev. Lett. 38 (1977) 1072.
[15] R.H. Dixon, J.F. Seely and R.C. Elton, Phys. Rev. Lett. 40 (1978) 122.
[16] E.Ya. Kononov, K.N. Koshelev, Yu.A. Levykin, Yu.V. Sidelnikov and S.S. Churilov, Sov. J. Quant. Electron. 6 (1976) 308.
[17] V.V. Korukhov, N.G. Nikulin and B.I. Troshin, Sov. J. Quant. Electron. 12 (1982) 1099.
[18] E.Ya. Kononov and K.N. Koshelev, Sov. J. Quant. Electron. 4 (1975) 1340.
[19] A.N. Zherikhin, K.N. Koshelev, P.G. Kryukov, V.S. Letokhov and S.V. Chekalin, Sov. J. Quant. Electron. 11 (1981) 48.
[20] W.E. Behring, R.J. Ugiansky and U. Feldman, Appl. Optics 12 (1973) 528.
[21] U. Feldman, J.F. Seely and A.K. Bhatia, At. Data and Nucl. Data Tables, to be published.
[22] A.K. Bhatia, U. Feldman and J.F. Seely, At. Data and Nucl. Data Tables, to be published.
[23] E.Ya. Kononov, A.N. Ryabtsev and S.S. Churilov, Phys. Scripta 19 (1979) 328.
[24] Bengt Edlen, Phys. Scripta 28 (1983) 51.
[25] R.L. Kelly, Atomic and ionic emission lines below 2000 Angstroms, Oak Ridge National Laboratory Report ORNL 5922 (1982).
[26] G.W. Erickson, J. Phys. Chem. Ref. Data 6 (1977) 831.
[27] G.V. Peregudov, M.E. Pistkin and E.N. Ragozin, Sov. J. Quant. Electron. 9 (1979) 1224.
[28] H.R. Griem, Milan Blaha and P.C. Kepple, Phys. Rev. A19 (1979) 2421.

Appendix II

Multibeam, laser-imploded cylindrical plasmas

M. C. Richardson, R. Epstein, O. Barnouin, P. A. Jaanimagi,* R. Keck, H. G. Kim,
R. S. Marjoribanks, S. Noyes, J. M. Soures, and B. Yaakobi
Laboratory for Laser Energetics, University of Rochester, 250 East River Road, Rochester, New York 14623-1299
(Received 20 September 1985)

Four orthogonal line-focused 351-nm beams have been used to implode 2-mm-long, 100-μm-diam thin Al cylinders. The resulting linear, high-density, high-temperature plasma has characteristics suitable as an x-ray-laser medium.

I. INTRODUCTION

Many proposed x-ray-laser schemes incorporate a linear, high-density, high-temperature plasma generated by a cylindrically focused beam, or by multiple spherically focused beams from a high-intensity laser.[1] For the plasma to be optimum as an x-ray-laser medium, it should not only have density and temperature conditions appropriate for maximum population of the x-ray-laser ion states, but also have a geometric shape and uniformity of plasma conditions conducive to providing high x-ray gain along the axis of the plasma. Most experimental studies of collisionally excited or recombination x-ray laser schemes have so far used laser-produced plasmas created from solid targets. The characteristics of such plasmas produced by spherically focused laser beams have been investigated in great detail because of their application to laser fusion studies. Plasmas created by cylindrically focused laser beams have not been examined so thoroughly.[2] In some respects, plasmas produced from solid massive targets by short intense laser pulses are not ideal for x-ray-laser schemes. These plasmas have steep electron-density and temperature gradients across which ion-state populations are rapidly varying, making the conditions for x-ray gain highly transient. In general the plasma flow in these high-laser-intensity interactions is not stationary, and as a consequence regions of specific ion-state populations are not stationary with respect to an optical axis through the plasma, thereby limiting the time for which optimum gain conditions exist. Moreover, refraction of x-rays on the plasma density profile can contribute to an additional loss. These factors are compounded by the microscopic variations produced in the plasma profile by the small-scale variations in the intensity profile of most focused laser beams. These limitations can be alleviated with simple changes to the target design.

One approach to producing a more uniform plasma in which the effects of nonuniformities in the irradiating beam are smoothed out is to form the plasma from an exploding thin foil. There are several ways in which a thin foil can be exploded or decompressed in the early stages of its irradiation by a high-power laser pulse. It is well-known that the interaction of intense ($>10^{14}$ W cm^{-2}) short (<100 ps) long-wavelength ($\lambda \gtrsim 1$ μm) laser radiation with solid material is dominated by resonance absorption,[3] a process in which most of the absorbed energy is coupled through intense electromagnetic plasma waves to collisionless fast, or hot, electrons. In a thin-foil interaction, these hot electrons quickly explode the foil by electron energy deposition. Similar conditions may be achieved with intense short-wavelength radiation where rapid decompression of the foil results from shock and radiational heating.[4] Alternatively, targets fabricated of low-density material ($n < n_{\text{solid}}$) may be good candidates for x-ray-laser media, although the effects of self-induced whole-beam self-focusing may have to be taken into account.[5]

II. IMPLODING CYLINDRICAL TARGETS

We describe here two novel approaches to the development of a linear uniform medium suitable for x-ray gain conditions. Both these approaches depend upon the ability to uniformly compress cylindrical targets with multiple, line-focused laser beams. In these initial investigations, we have considered primarily Al cylinders for a number of reasons. The spectroscopy of Al is well-known,[6] and there are a number of transitions on which high gain can potentially be produced in a recombining plasma,[7,8] with or without enhanced plasma cooling.[8] With the limited energy currently available under line-focus conditions with OMEGA, we consider the implosion of cylinders of moderate Z, in which temperatures sufficiently high to ionize and excite the requisite energy levels can be generated (typically >400 eV). Thirdly, we chose Al because of its relative ease of fabrication in the form of free-standing, ultrathin-walled cylinders.

In this paper, we present some initial investigations of these ideas performed with four line-focused beams of the upconverted 351-nm OMEGA facility.[9] The four beams, each producing ≈ 50 J in ≈ 600 ps, were focused orthogonally onto the cylindrical target (Fig. 1) by an $f/3.7$ fused-silica lens combination comprising a high-power aspheric singlet lens and a close-coupled spherical cylindrical corrector plate, producing a line focus of length 1700 μm and width $\gtrsim 50$ μm. Focused onto a target of ≈ 100-μm diameter, with the four beams tangentially overlapping the target, average irradiation intensities of $\sim 10^{14}$ W/cm^2 were produced. The four beams were coaligned with the aid of a solid reflective cylindrical surrogate target, from which fiducials were transposed to fixed high-resolution viewing systems for positioning the irradiated

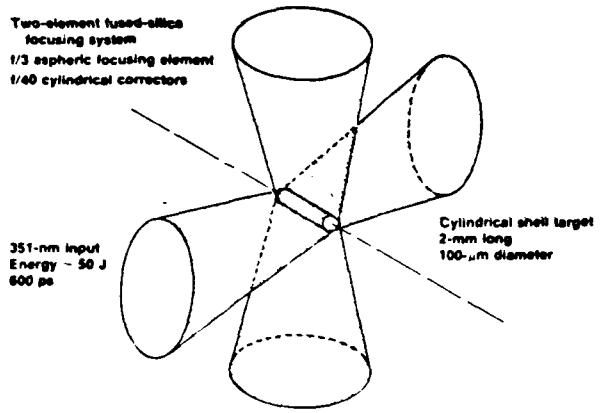

FIG. 1. Four-beam compression of cylindrical targets with orthogonal 351-nm line-focused beams of OMEGA.

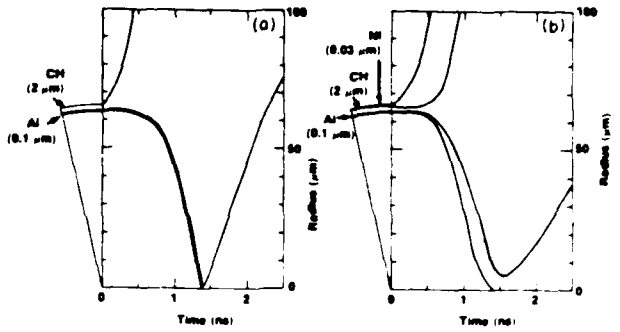

FIG. 3. Trajectories of material interfaces predicted by the one-dimensional hydrocode LILAC for the ablation target shown in Fig. 2(a). (a) shows the case for a low-Z center ablator, (b) shows the effect of adding a thin layer of high-Z material (Ni).

targets. Individual beams were aligned in position to an accuracy of $\approx 20\,\mu$m, and oriented parallel to one another to $\sim 10^{-2}$ rad. For the purpose of aligning the cylindrical plasma to the axis of diagnosing instrumentation, the axis of the cylindrical target could be set to an axis fixed to the enclosing vacuum chamber to an accuracy of 3×10^{-3} rad.

Two types of imploding targets were investigated, and compared to a solid Al cylinder target. These are illustrated in Fig. 2. The first, Fig. 2(a), comprised a 100-μm-diam CH cylindrical shell, 3–5 μm thick, the inside of which was coated with a 0.3-μm-thick layer of Al. The CH in this target serves as an ablator, its thickness being chosen to equal the ablation depth for an intensity of $\sim 10^{14}$ W/cm^{-2}.[10] Thus the Al layer is subjected to minimal heating until it stagnates at the center of the target. One-dimensional hydrodynamic simulations of this type of target with the Lagrangian code, LILAC (Fig. 3),[11] indicate that the Al reaches final density and temperature conditions of 4×10^{24} cm^{-3} and ≈ 300 eV, respectively, over a radial extent of $\lesssim 3\,\mu$m. Being ablatively driven by short-wavelength radiation, this target is sensitive to irradiation nonuniformities resulting from the use of only four beams. Were this final core density to be created it would be somewhat higher than the optimum for most soft-x-ray-laser schemes, and persists for only a short period of time. However, it is unlikely that the sharp central peak in density predicted by the one-dimensional hydrocode would, in reality, materialize. Some excursions from a uniform implosion would smooth the sharp density peak into the surrounding plasma. These conditions can in any case be modified by the addition of a thin ($\approx 0.015\,\mu$m) high-Z (Au) radiational source of preheat on the outside of the CH shell. The initial burst of x-ray emission from the Au shell penetrates the CH and preheats the Al before it is compressed. The resulting in-flight decompression of the Al leads to a reduced final core density. Although the temperature of the preheated target is reduced to ≈ 130 eV, the effect of the radiation from the outer layer is to increase (almost threefold) the duration over which the Al maintains a temperature in excess of 100 eV, to decrease the final core density by a factor ≈ 3 and to increase the spatial extent of the predicted central density peak to $\approx 10\,\mu$m.

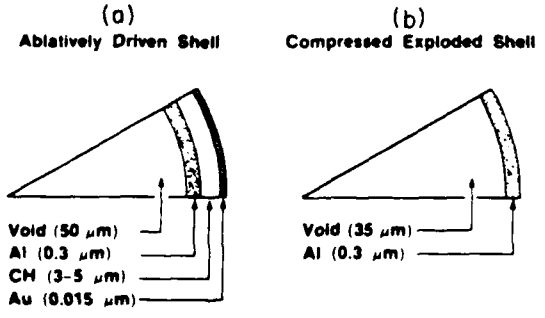

FIG. 2. Two types of cylindrical target designs investigated (a) a CH-coated metal cylinder, in which the CH acts as an ablator; (b) an ultrathin metal cylinder which explodes before being compressed.

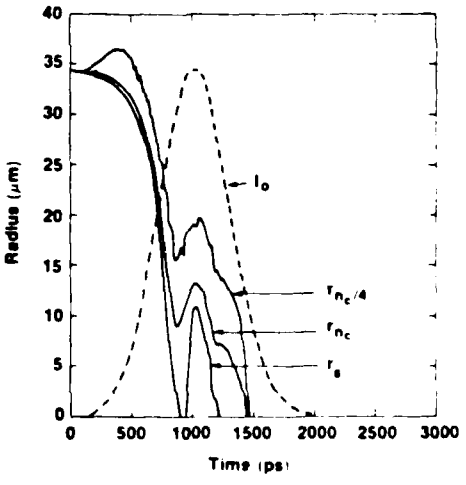

FIG. 4. One-dimensional simulation of the decompression and implosion of an ultrathin-walled metal (Al) cylindrical shell target.

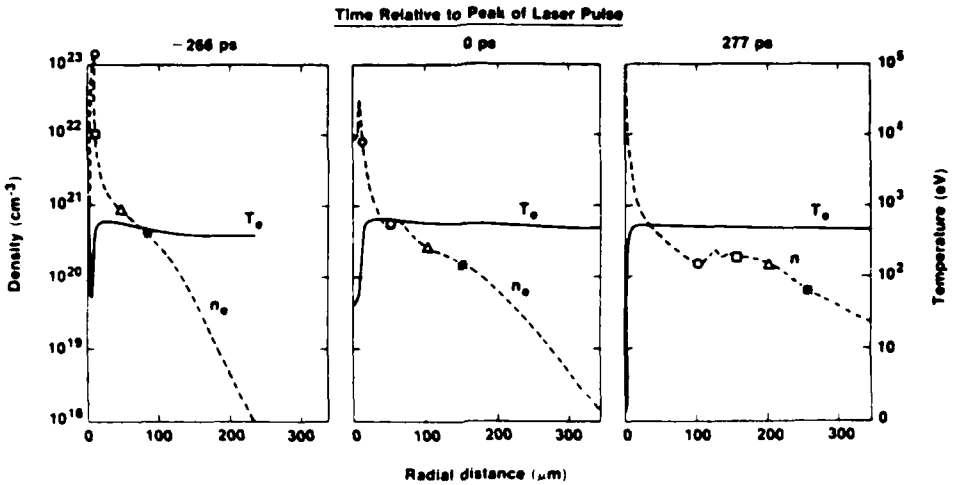

FIG. 5. Density and temperature profiles at different times following the implosion of a thin Al cylindrical shell of the type shown in Fig. 2(b).

The second type of cylindrical target is shown in Fig. 2(b). This consists of an ultrathin (0.3 μm) Al cylinder, ≈ 70 μm in diameter.[12] The target is fabricated by a novel method in which a solid cylinder of polystyrene is first overcoated with a thin layer of Al, and then leached away by chemical etching.[12] LILAC hydrocode simulations indicate that when irradiated, the thin Al cylindrical shell rapidly decompresses, reaching a mass-averaged density of $\approx 0.1 n_{\text{solid}}$, at a time ≈ 500 ps before the peak of the laser pulse (Fig. 4). The decompressed shell then rapidly implodes, producing at stagnation a small (≈ 30 μm diameter) high-density region in the center of the cylinder, surrounded by a lower density plateau (Fig. 5). A fairly large fraction (see Fig. 5) of the mass of the original shell is located in the high-density central region. In the post stagnation phase, this central high-density region unloads radially and aids in maintaining the long scale length of the electron density plateau. In Fig. 5, this phenomenon can be seen by following the outward flow of the Lagrangian cell marks with time. From Fig. 5, it can be seen that two regions of the plasma possess parameters suitable as an x-ray-laser medium. The narrow central region reaches electron densities higher than 10^{22} cm^{-3} over a radial extent of 10–20 μm with a temperature of several hundred electron volts. Although the code predicts a minimum in the electron temperature on axis, it is likely that in reality, the temperature in this region would be smoothed by small scale inhomogeneities. This high-density, high-temperature region persists for some time (several 100 ps) following the implosion, and therefore offers potentially an optimal medium for x-ray amplification. The underdense region of the plasma is maintained by flow of plasma from the dense core. Under the influence of continuing absorption during the remainder of the laser pulse, a long, radially expanding plateau of plasma of electron density larger than 10^{20} cm^{-3} is produced. Almost stationary in profile, and with an electron temperature approaching 1 keV, this plasma provides conditions generally considered optimum for collisional excitation or recombination pumped laser schemes.

III. EXPERIMENTAL INVESTIGATIONS

In order to test these concepts, exploratory experiments were made with cylindrical targets irradiated by four orthogonal, line-focused uv (351-nm) beams from the 24-beam OMEGA laser facility. The primary intent behind these investigations was to examine experimentally the target concepts described above with a view to determining the degree to which these implosions are one-dimensional (or geometrically uniform), and to what extent the code correctly predicts the plasma conditions.

Several experiments were performed with targets of the type illustrated in Fig. 2, and compared with uniformly irradiated solid Al cylindrical targets of the same diameter. An extensive array of diagnostics was deployed in these experiments (Fig. 6), including plasma calorimetry, x-ray photography, and time-integrated x-ray spectroscopy. Time-resolved x-ray measurements were made with two instruments, an x-ray transmission grating spectrograph coupled to a streak camera,[13] and an elliptical crystal spectrograph also coupled to a streak camera.[14]

Absorption was measured with an approximately isotropic array of 20 plasma calorimeters. These registered a uniform plasma blow-off distribution, with overall absorption of $\approx 50\%$ for the solid and ablatively driven

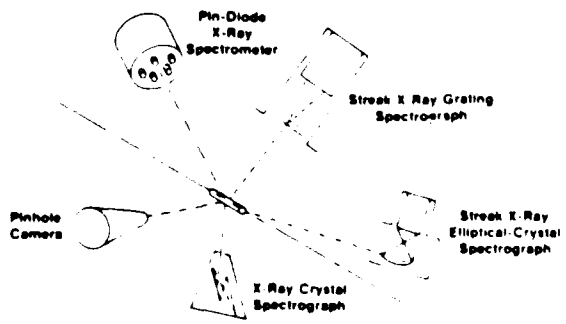

FIG. 6. Schematic of principal diagnostic systems deployed to characterize cylindrical plasma.

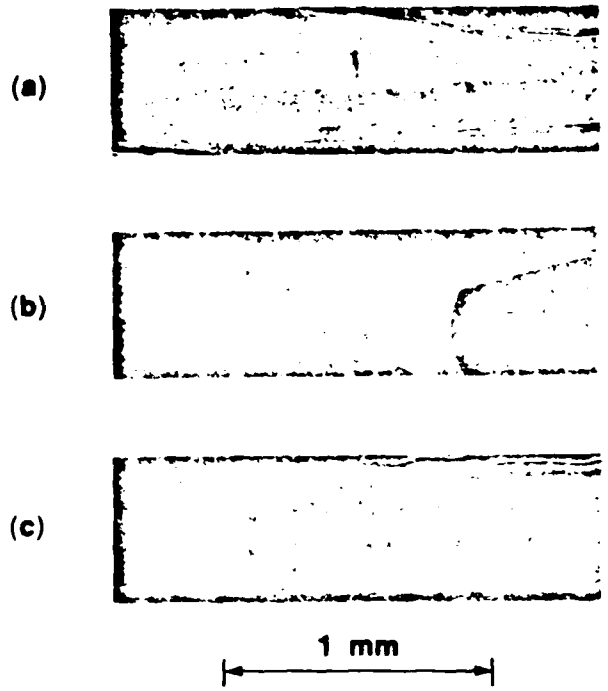

FIG. 7. X-ray pinhole photographs of cylindrical Al targets. (a) shows that of a solid Al target of 125 μm diameter, (b) an ablative target of Al type shown in Fig. 2(a), and (c) an ultrathin Al cylinder of ≈ 75 μm diameter.

cylinders, and typically $\approx 44\%$ for the thin Al cylinders. These measured values of absorption are to be compared to those predicted by the LILAC hydrocode. These one-dimensional simulations assumed an $f/3.5$ cylindrical focusing geometry of beams focused 6 target radii beyond the target center. Account is taken for refraction of the beam in the plasma. The overall corona absorption predicted by LILAC was $\approx 57\%$ for the thin Al cylindrical targets and $\approx 98\%$ for the solid and ablatively driven targets. The latter value is comparable to that predicted and measured for solid spherical targets with 351-nm radiation at a similar intensity.[15] The somewhat lower measured values may be the result of a greater fraction of the laser energy being in the wings of the intensity distribution with cylindrical optics. Apart from x-ray photographic studies of the extent of the line focus, no optical measurements of the focal distribution have been made. In a previous study of line focus conditions,[2] an intensity distribution in the focal plane was measured in which about half of the energy resided in a broad, low-intensity plateau surrounding the main line-focused region.

X-ray image data of those types of targets irradiated is shown in Fig. 7. These were obtained with a pinhole x-ray camera (10-μm pinhole) in a 25-μm-thick Be filter, producing images in the 0.8–1.5-keV range. The x-ray image of the solid Al target [Fig. 7(a)] indicates qualitatively the apparent uniform illumination of the target in cylindrical geometry. Figure 7(b) shows the x-ray image of an ablatively driven Al shell. This particular target had an outer layer of Au; however, little difference in the x-ray emission from the target was observed if there was no Au layer. Weak x-ray emission from the core of the imploded shell can be observed. However, its uniformity along the 2-mm length of the target is poor, as is the linearity of the compressed core. Figure 7(c) shows the x-ray image of a compressed thin Al (0.3-μm) shell. The resulting x-ray emission is uniform and collinear with the original cylinder axis, and its radial extent (≈ 25 μm diameter) is in good agreement with the LILAC predictions. Details of this image are shown in Fig. 8 which shows the

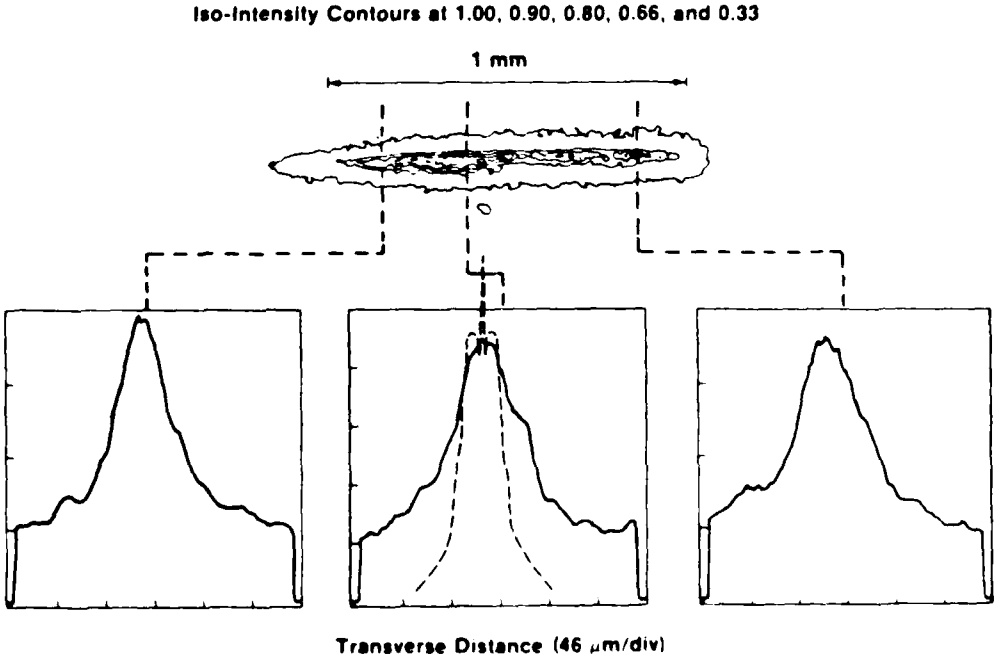

FIG. 8. Calibrated reduction of the x-ray image of the imploded ultrathin Al cylinder.

calibrated intensity of the x-ray emission, together with a LILAC prediction of the spatial extent of x-ray emission. Bright x-ray emission originates from a uniform linear core of $\approx 20\ \mu$m in radial extent. This is then surrounded by an annular region of 100 μm radial extent. Qualitatively this is similar to the predictions of the one-dimensional LILAC simulations shown in Fig. 5, which indicate the formation of a narrow high-density central compressed core unloading into a broader lower-density plateau.

The overall relative x-ray conversion was measured with the low-energy channels ($E < 3$ keV) of a 15-channel, K-edge-filter p-i-n diode–photomultiplier-scintillator x-ray continuum spectrometer. Assuming isotropy of x-ray emission, the total low-energy x-ray intensity from the CH ablative target, the Au-coated ablative target, the thin Al target, and the solid Al target were in the ratio 0.02:0.1:1.3:1.0.

Time-integrated x-ray spectra of Al emission were recorded with two planar crystal spectrographs situated coaxial and orthogonal to the axis of the cylindrical target axis. Each spectrograph employed a gypsum crystal ($2d = 15.15$ Å), and surveyed a spectral region of 6.6–8.0 Å. Spectra were recorded on Kodak RAR-2497 film developed according to the calibration of this film by Henke *et al.*[16] Figure 9 shows details of these spectra. The temperature of the emitting region was estimated from the ratio of the intensities of the Al Lyman α (7.173 Å) and the Al Heβ ($1s^2$-$1s3p$) at 6.635 Å. The latter transition is less sensitive to reabsorption than the Heα ($1s^2$-$1s2p$) transition. Assuming an optically thin plasma for the spectra observed orthogonally to the cylinder axis, and with the assumption of a collisional-radiative model,[17] a temperature of 600–700 eV is deduced.

Time-resolved x-ray spectroscopic studies of the x-ray emission from the line plasma were made with two streak spectrographs. These two instruments complemented one another in spectral resolution and range. The first of these instruments was a streak transmission grating spectrograph[13] which provided modest spectral resolution (1.5 Å) over a broad spectral range (1–30 Å), with a time resolution of ≈ 30 ps. This spectrograph observed x-ray emission was orthogonal to the cylinder axis and comprised a free-standing, 0.6-μm-thick, Au bar-grating with an interbar period of 3000 Å, in conjunction with a streak camera having a soft-x-ray-sensitive CsI photo-

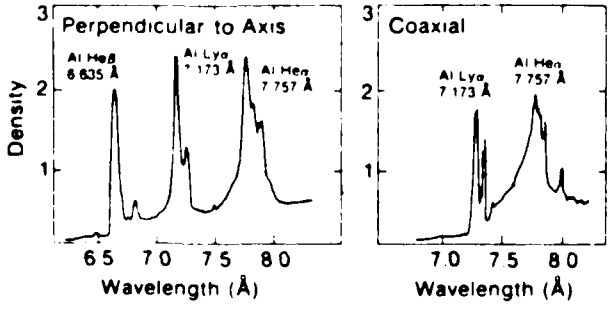

FIG. 9. Time-integrated x-ray spectra obtained collinear and orthogonal to the cylinder axis.

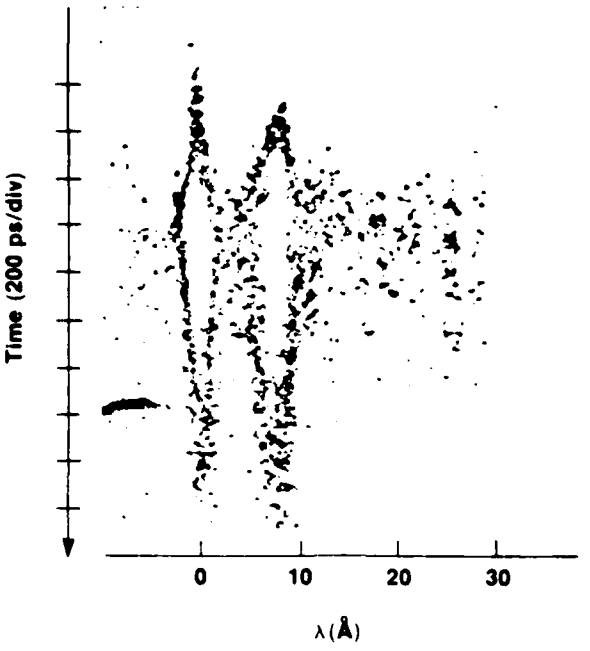

FIG. 10. Time-resolved soft-x-ray spectra from the streak transmission grating spectrograph. Data are those from an imploding ultrathin Al cylindrical target.

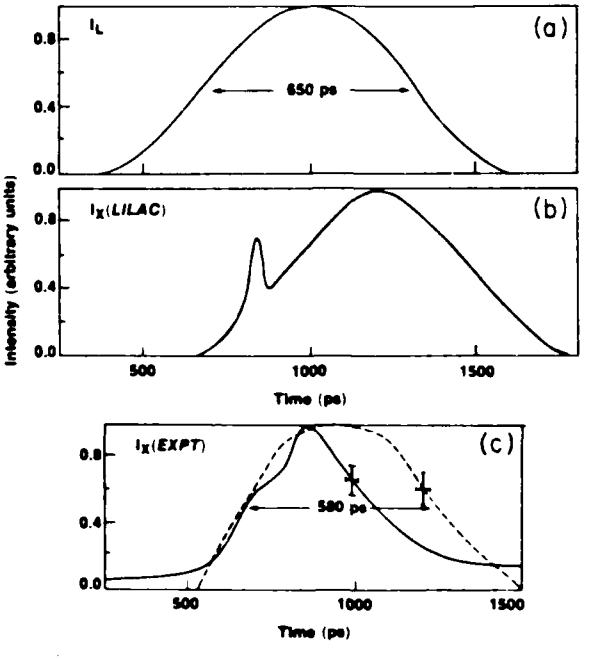

FIG. 11. Comparison of a time-resolved soft-x-ray data with predictions from LILAC. (b) shows the predicted x-ray emission in the range 1.5–2.2 keV compared to the duration of the laser pulse (a). (c) shows the measured shape of the x-ray emission in the 1.5–2.2-keV range (solid line) and the measured overall x-ray emission (dotted). No direct time relation was established between the x-ray emission and the laser pulse.

cathode (100 nm thick) deposited on a 70-nm-thick Formvar film overcoated with a 30-nm layer of Au. A typical time-resolved spectrogram of the compressed cylindrical plasma is shown in Fig. 10. The two-dimensional image recorded by the streak spectrograph was digitized and processed to remove image nonlinearities introduced by pin-cushion distortion in the streak camera image intensifier, and a nonlinear streak rate in the electron-optical deflection circuitry. The recorded emission is dispersed chiefly in the first order of the grating and shows the durations of the continuum emission and of the unresolved He-like and H-like Al resonance lines. Figure 11 shows the history of the x-ray emission as predicted by the one-dimensional hydrodynamic code post processed by a non-LTE (non–local-thermodynamic-equilibrium) model of ionization, together with representative experimental data recorded with the streak grating spectrograph. Figure 11(b) shows the predicted x-ray intensity in an x-ray window of 1.5–2.2 keV, approximately that region in which the resonance line emission from Al would fall on a time scale similar to that of the laser pulse, Fig. 11(a). A clear peak in the emission is obtained, corresponding to the time at which the decompressed shell stagnates at the center of the cylinder. This peak in x-ray emission is superimposed on top of a broad x-ray signal having a duration similar to the laser pulse. The second peak in x-ray emission observed in Fig. 11(b) coincides with the peak in the average temperature of the plasma, and also with the rebound compression in the compressed target, as indicated in Figs. 4 and 5. Typical temporal records of x-ray emission recorded from the streak grating spectrograph are shown in Fig. 11(c). The dotted trace shows the time history of all the x-ray radiation in the range 0.6–4.0 keV, and has a smoothly varying envelope of duration similar to the laser pulse. The solid curve shows the temporal shape of the emission in the range 1.5–2.2 keV, bracketing that region in which the resonance lines are emitted. In this trace, a sharp peak in the emission is observed, which could be interpreted as being due to the initial compression of the shell.

High-resolution time-resolved spectrograms of He-like and H-like Al resonance lines were recorded on a second streak spectrograph. This instrument provided high-resolution ($\lambda/\Delta\lambda \approx 600$) time-resolved spectra in the range 5–7 Å (1.77–2.48 keV) with a time resolution of 10 ps. This device consisted of a calibrated, elliptically curved PET (pentaerythritol) crystal combined with a second x-ray streak camera having a photocathode of CsI (120 nm thick) deposited onto a 12.7-μm Be substrate.[14] Typical

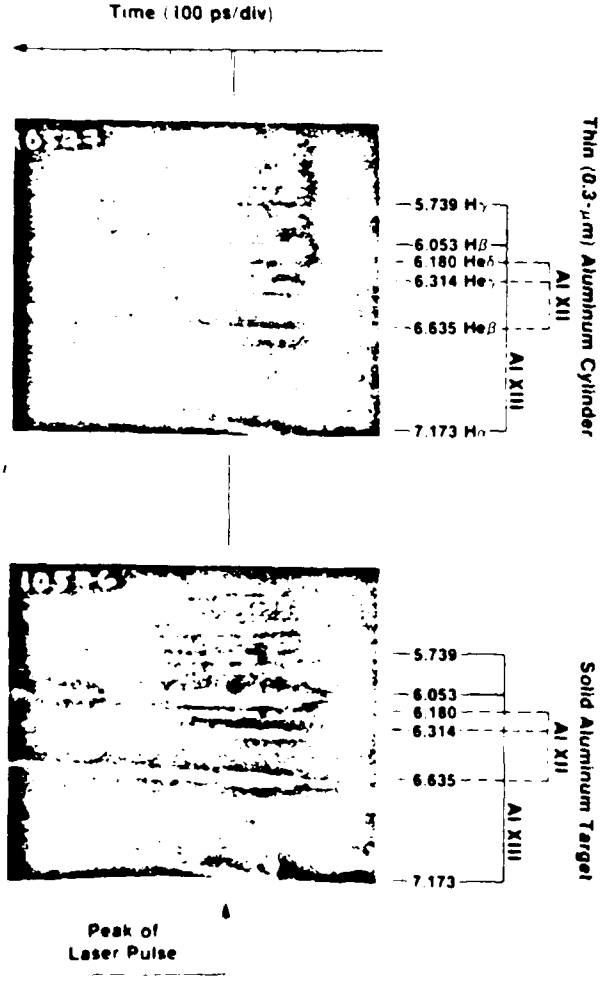

FIG. 12. Time-resolved x-ray spectra of Al resonance lines from ultrathin shell and solid targets.

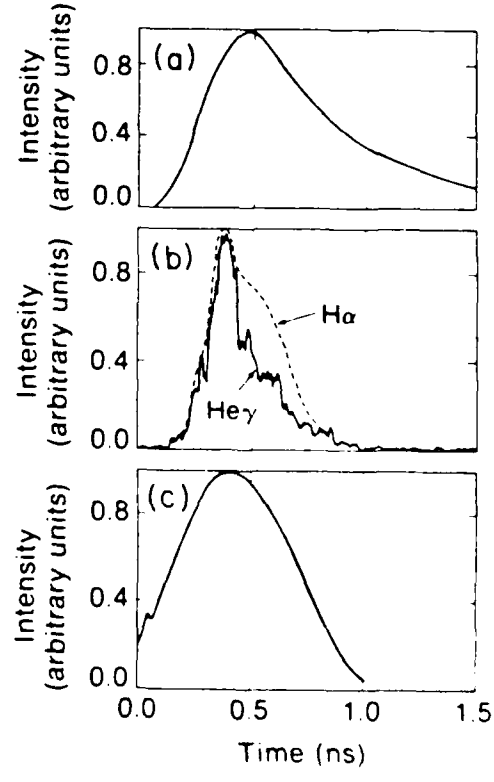

FIG. 13. Time profiles of the x-ray emission. (a) from the solid target; (b) from the Al shell target Al $1s$-$2p$ line (– – –), Al $1s^2$-$1s4p$ line (——); and (c) non-LTE simulation of the Al $1s$-$2p$ line intensity.

time-resolved spectra from this instrument are shown in Fig. 12. Figure 12(a) shows the spectra from a compressed cylindrical target, while that in Fig. 12(b) shows the duration of Al emission from the plasma off a solid Al rod target. Both the He-like and H-like lines can clearly be resolved, as well as the recombination emission at higher x-ray energies. The slight inward distortion in the streaked lines is due to an artifact in the streak tube. Figure 13 shows reduced data obtained from these streak spectrograms. Figure 13(a) shows the time duration of the integrated spectral emission in the 5–7.5 Å range recorded from the solid cylindrical target. The shape and duration of the emission is typical of the x-ray emission from the corona from a solid metallic target. In Fig. 13(b) is shown the time history of specific lines emanating from the compressed cylindrical target. The dotted line shows the duration of the Hα line whilst the solid line shows the time history of the Heγ line of Al. The overall duration of these individual lines is significantly shorter than the laser pulse and the x-ray emission which results from the coronal plasma produced off a solid target. The Hα line emission predicted by the non-LTE post processor is shown in Fig. 13(c) and is seen to be similar to the observed emission in duration and, to some extent, in shape. The peak in the simulated emission corresponds with the peak in the average temperature of the plasma. The differences in the detailed shapes of the observed and simulated emission histories may be related to effects causing the differences between the observed and simulated emission in Fig. 11, but the specific connection is not clear. The integration of the Heβ and Hβ lines and the comparison of their overall relative intensities provides an estimate of ≈ 500 eV for the averaged plasma temperature, in reasonable agreement with the predicted value.

IV. SUMMARY

This initial investigation of the plasma created by imploding cylindrical targets has provided some interesting data from which future studies can optimize the production of linear plasmas suitable as x-ray-laser media. From the present studies it is clear that thick ablatively driven cylindrical shells will only implode symmetrically under illumination conditions more uniform than used in these investigations. However, the submicron-thick metallic shells, which rapidly decompress upon irradiation, implode symmetrically to produce conditions which appear to be similar to these predicted by the one-dimensional code LILAC. Further studies are planned to examine in detail the production of specific atomic levels during shell implosions.

ACKNOWLEDGMENTS

The authors wish to acknowledge discussions with J. Delettrez, R. L. McCrory, S. Skupsky, and C. P. Verdon at the Laboratory for Laser Energetics; U. Feldman and J. Seely at the U.S. Naval Research Laboratory; and D. C. Matthews and M. Rosen at Lawrence Livermore National Laboratory. This work was supported by the U.S. Department of Energy Office of Inertial Fusion under agreement No. DE-FC08-85DP40200 and by the Laser Fusion Feasibility Project at the Laboratory for Laser Energetics which has the following sponsors: Empire State Electric Energy Research Corporation, General Electric Company, New York State Energy Research and Development Authority, Northeast Utilities Service Company, Ontario Hydro, Southern California Edison Company, The Standard Oil Company, and the University of Rochester.

---

*Permanent address: Lawrence Berkeley Laboratory, University of California, Berkeley, CA 94720.

[1]For a general review of the short-wavelength laser approach, see R. W. Waynant and R. C. Elton, Proc. IEEE **64**, 1058 (1976); F. V. Bunkin, V. I. Derzhiev, and S. I. Yakovlenko, Kvant. Elektron. (Moscow) **8**, 1621 (1981) [Sov. J. Quantum Electron. **11**, 981 (1981)].

[2]M. D. J. Burgess, R. Dragila, B. Luther-Davies, K. A. Nugent, A. J. Perry, G. J. Tallents, M. C. Richardson, and R. S. Craxton, Phys. Rev. A **32**, 2899 (1985).

[3]D. W. Forslund, J. M. Kindel, K. Lee, E. L. Lindman, and R. L. Morse, Phys. Rev. A **11**, 679 (1975); K. G. Estabrook, E. J. Valeo, and W. L. Kruer, Phys. Fluids **18**, 1151 (1975).

[4]Y. B. Zeldovich and Y. P Raizer, *Physics of Shock Waves and High Temperature Hydrodynamic Phenomena* (Academic, New York, 1966), Vol. 1.

[5]H. Figueroa, C. Joshi, C. E. Clayton, H. Azecchi, H. A. Ebrahim, and K. A. Estabrook, in *Laser Interaction and Related Plasma Phenomena*, edited by G. Miley and H. Hora (Plenum, New York, 1984), Vol. 6, p. 527.

[6]R. L. Kelly and L. V. Palumbo, U.S Naval Research Laboratory Report No. 7599, 1973 (unpublished).

[7]P. Jaegle, A. Carillon, P. Dhez, G. Jamelot, A. Sureau, and M. Cukier, Phys. Lett. **36a**, 167 (1971).

[8]Y. Contune, B. Yaakobi, J. Delettrez, and J. M. Forsyth, in *Laser Techniques for Extreme Ultraviolet Spectroscopy (Boulder, 1982)*, edited by T. J. McIraith and R. R. Freeman (AIP, New York, 1982), p. 312.

[9]J. M. Soures, R. J. Hutchison, S. D. Jacobs, L. D. Lund, R. L. McCrory, and M. C. Richardson, *Proceedings of the Tenth Symposium on Fusion Engineering, Philadelphia* (IEEE, New York, 1983), p. 1392.

[10]B. Yaakobi, O. Barnouin, J. Delettrez, L. M. Goldman, R. Marjoribanks, R. L. McCrory, M. C. Richardson, and J. M. Soures, J. Appl. Phys. **57**, 4354 (1985).

[11]These simulations were run assuming ray tracing and collisional absorption of cylindrical irradiation, classical thermal transport with flux inhibition ($f=0.045$), SESAME equation-of-state tables [B. I. Bennett, J. D. Johnson, G. I. Kenley, and G. T. Rood, Los Alamos National Laboratory Report No. LA-7130, 1978 (unpublished)], and multigroup radiation transport using tabulated LTE opacities [W. F. Heubner, A. L. Merts, N. H. Magee, and M. F. Argo, Los Alamos National Laboratory Report No. LA-6760, 1977 (unpublished)], Rosseland-averaged over each photon-energy group. The non-LTE simulations involve re-solving the radiation problem for the n_i, T_e, information from a LILAC run using opacities and emissivities from atomic populations obtained from rate equations [R. Epstein, S. Skupsky, and J. Delettrez, J. Quant. Spectrosc. Radiat. Transfer (to be published)].

[12]H. Kim, S. Noyes, M. C. Richardson, and B. Yaakobi, J. Vac. Sci. Technol. (to be published).
[13]M. C. Richardson, R. S. Marjoribanks, S. A. Letzring, J. M. Forsyth, and D. M. Villeneuve, IEEE J. Quantum Electron. QE-19, 1861 (1983).
[14]B. L. Henke and P. A. Jaanimagi, Rev. Sci. Instrum. 56, 1537 (1985).
[15]M. C. Richardson, R. S. Craxton, J. Delettrez, R. L. Keck, R. L. McCrory, W. Seka, and J. M. Soures, Phys. Rev. Lett. 54, 1656 (1985).
[16]B. L. Henke, F. G. Fujiwara, M. A. Tester, C. H. Dittmore, and M. A. Palmer, J. Opt. Soc. Am. B 1, 828 (1984).
[17]R. H. Huddlestone and S. L. Leonard, *Plasma Diagnostic Techniques* (Academic, New York, 1965), Chap. 5, p. 29.

Appendix III

Fabrication of thin cylindrical targets for x-ray laser experiments

H. Kim, S. Noyes, M. C. Richardson, and B. Yaakobi
Laboratory for Laser Energetics, University of Rochester, Rochester, New York 14623-1299

(Received 26 September 1985; accepted 15 November 1985)

For a laser-produced plasma to be most useful in current x-ray laser experiments, it should have a cylindrical shape and a uniform plasma density and temperature to provide high x-ray gain along the axis. One approach to producing such a plasma is the uniform compression of hollow cylindrical targets with multiple, line-focused laser beams. These targets are typically ultrathin (<3000 Å) cylindrical shells of materials such as Al. These cylinders have diameters $\simeq 100\,\mu$m and lengths $\simeq 2$ mm. To fabricate such targets, solid polystyrene cylinders are coated with a metal and/or parylene layer of the appropriate thickness. The coated cylinder is then cut to the desired length and the polystyrene is leached out by immersing the system in a solvent.

I. INTRODUCTION

There is considerable interest in x-ray laser schemes which incorporate collisional or recombinational pumping. Gains on selected transitions of Se and Y neon-like ions have recently been reported for a collisionally pumped system utilizing ultrathin (750 Å) foils supported on thin Formvar substrates.[1] In addition, gain on the 182 Å transition of C VI has been reported in recombination laser schemes from solid wires,[2] and thin foil targets.[3]

An optimum laser medium for collisional scheme is a uniform, high aspect ratio plasma of electron density 10^{20}–10^{21} cm^{-3} and temperatures in excess of 500 eV. X-ray refractory losses from the medium will be minimized with a low transverse electron density gradient in the plasma, and laser output will increase, the longer these conditions are maintained. In a theoretical and experimental study at the Laboratory for Laser Energetics (LLE), University of Rochester, selected target geometries have been investigated to optimize these parameters. One target geometry which appears to have some advantages over planar foil targets is a thin-walled cylindrical target. When irradiated with orthogonally oriented, line focused laser beams, as can be provided by the OMEGA facility at LLE, the wall of the target uniformly compresses, before being imploded to form a hot dense linear plasma.[4] Subsequent to the cylinder implosion, the lateral plasma density profile becomes flat-topped and broad; this leads to reduced refraction losses of the x-ray laser even with a relatively long lasing medium. Prior to peak implosion, the lateral density profile has a minimum on axis; x-ray laser refraction now can be beneficial in that it causes collimation. Figure 1 illustrates such an experimental geometry.

This paper describes the fabrication technique for these ultrathin metallic cylindrical shells.

II. FABRICATION OF CYLINDRICAL TARGETS

The cylindrical target to be fabricated is schematically illustrated in Fig. 2. The method of fabrication is similar to that[5] which we have developed for fabricating high-aspect-ratio, plastic-coated, metal-shell inertial fusion targets. The fabrication steps are illustrated in Fig. 3. The sequence begins with the selection of a polystyrene fiber of proper diameter. Coiled (or otherwise not straight) fibers are straightened by drawing them in a water bath at its boiling temperature. The fibers are cut to about 1.5 cm and perpendicularly bonded to a glass stalk at their midpoints. The fiber is next coated with aluminum using magnetron sputtering.[6] In magnetron sputtering, we have utilized a pulsed nitrogen process[7] to obtain an excellent surface finish. This metal sputter coating should be performed at temperatures below the glass-transition temperature of polystyrene, 90 °C, to prevent deformation of the polystyrene mandrel. The aluminum coating is then followed by a parylene coating. After coating, the fibers are cut to a 2 mm length using a specimen grid trimmer made by E. F. Fullam, Inc. Fracture of the coated film at the point of shear was small (~ 5-μm chips) by this process. The coated fibers are placed in toluene at room temperature for 24 h during which the polystyrene cylinder is dissolved and leached out through both ends of the tubule. The resulting hollow cylinders are removed using an eye dropper and allowed to dry on a microscope slide. The targets are then mounted on drawn glass capillaries using UV curing epoxy.

The polystyrene was Dow Styron 685-*n*-26W which has a weight-average-molecular weight of 50 000. The polystyrene resin was extruded through a $\frac{3}{4}$-in. Brabender extruder

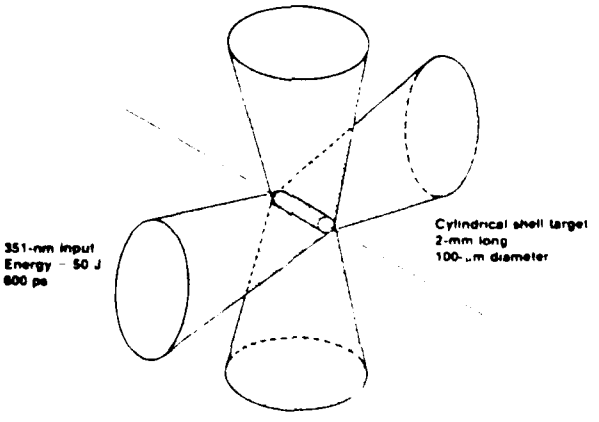

FIG. 1. Schematics of four beam compression of cylindrical targets with four orthogonal, line-focused beams of OMEGA laser system at LLE.

 0734-2101/86/031142-03$01.00

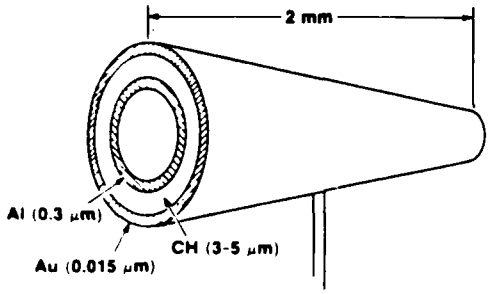

FIG. 2. Structure of cylindrical shell targets for x-ray laser experiments.

which had a temperature profile of 190 and 260 °C zones. The melted polystrene was then extruded through a 1.25-mm spinneret hole and melt stretched with a 15:1 ratio to form a 100-μm fiber.[8] In bonding the polystyrene fiber to a glass stalk, UV-cured epoxy proved to be a more suitable adhesive than RTV. Due to the the thermosetting nature of the UV-cured epoxy, the volume expansion of the epoxy upon being dissolved by the solvent is minimal and this contributes to the stability of the bonding even if it is immersed in a solvent during the leaching procedure.

The Al layer was coated on the polystyrene fiber by magnetron sputtering. Deformation of the fiber by the plasma heat can be avoided by positioning the fiber 10 cm from the sputter target. The optimum power density not to deform the polystyrene mandrel was 2–3 W/cm^2. Nitrogen gas pulsing during the sputter coating produced a very smooth surface finish.[7,9] The flow rate of Ar sputter gas was 3.0 sccm and the flow rate of N_2 was also 3.0 sccm during the nitrogen pulsing period. The pulsing rate was s in 3-min intervals. Without N_2 pulsing, the oblique incident of the flux of sputtered aluminum atoms causes self-shadowing, surface roughness, and voids, thus forming brittle coatings. Furthermore, columnar growth, a characteristic crystal-growth habit during thin-film depositions, also contributes substantially to the poor surface finish and inferior mechanical properties. When nitrogen ions, which can be considered defect forming impurities, are periodically injected onto growing crystallographic planes, they poison the growth. Therefore, ordinary dendritic crystallization cannot proceed. Deposit of nitrogen ions may become new heterogeneous nucleation sites. Under such conditions, either grain

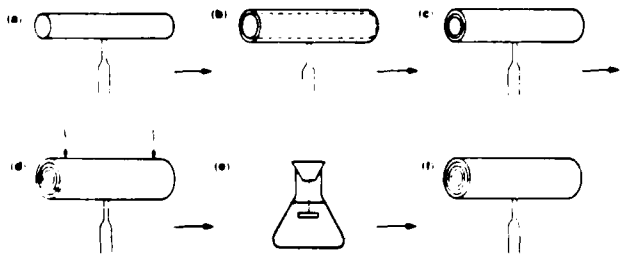

FIG. 3. Sequence for fabricating thin-walled large-aspect-ratio cylindrical targets. (a) Stalk-mount polystyrene fiber, (b) coat polystyrene fiber with metal layer in magnetron sputter, (c) coat polystyrene fiber with parylene, (d) cut to a desired length with a razor blade, (e) immerse in toluene to dissolve polystyrene, (f) remove tubule after 24 h. Target is fabricated.

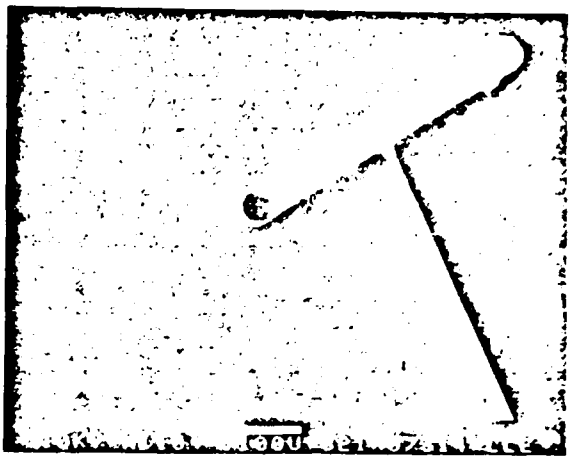

FIG. 4. Scanning electron micrograph of a thin-walled cylindrical aluminum shell.

refinement occurs or an amorphous structure forms. It has been shown that the structure obtained by nitrogen pulsing is essentially amorphous and the improved surface finish is due to the amorphous nature of the coating.[7] The Al coating was then followed by a parylene coating.[10] The coating process was closely monitored using optical reflectometry, which enables us to control the coating thickness to 500 Å.[11] In the parylene coating, only nonsubstituted 2, 2-paracyclopane was used, resulting in a relatively rough surface finish.[12] However, no complications are expected in using ethyl-substituted 2, 2-paracyclopane to obtain a smoother surface.[10]

III. DISCUSSION

The hollow cylindrical targets used for x-ray laser experiments which were fabricated by the above described procedure were characterized by scanning electron microscopy. For some experiments which utilized aluminum cylindrical shells, the parylene coating process was omitted. Figure 4 shows an SEM photo of such a target. As mentioned previously, the aluminum shell was fabricated by sputter coating of aluminum using a N_2 pulsing process.[7] The nitrogen gas pulsing incorporates a minute quantity of nitrogen atoms into the Al layer. Though the injection of nitrogen gas is by periodic pulsing, it is not an abrupt "on" and "off" switching

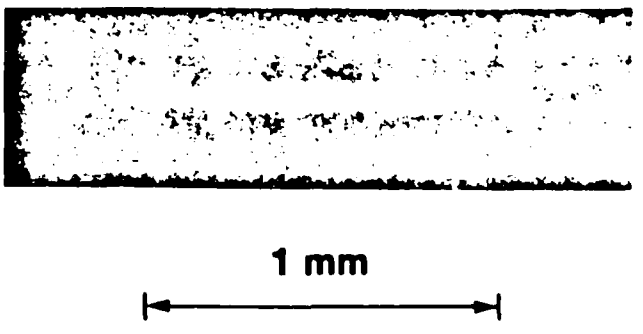

FIG. 5. X-ray photograph of a 3000 Å thin aluminum shell of 70 μm diameter irradiated by four orthogonal beams of the OMEGA laser system.

but resembles a sinusoidal shape. The net result is that nitrogen incorporation is more or less continuous. The uniform distribution of the nitrogen in the aluminum layer poisons the crystal growth in the layer and the film becomes amorphous. The chemical composition of the Al layer obtained by N_2 pulsing was studied by an energy dispersive x-ray analysis method and the content of nitrogen incorporation is estimated to be less than 5 at. %.

The cylindrical aluminum shell targets have been utilized in a recent experiment designed to produce linear plasmas suitable for x-ray laser media. The implosion of 3000 Å-thick Al shells 70 μm in diameter has generated x-ray emission (0.8–1.2 keV) which is uniform and collinear with the original cylinder axis, and whose radial extent ($\sim 25\,\mu$m diameter) is in reasonable agreement with hydrocode calculation. An x-ray photograph of the implosion is shown in Fig. 5. Detailed discussion of the experiment is described elsewhere.[4]

ACKNOWLEDGMENTS

Assistance by Dr. P. Park of Mobil Chemical Company, Macedon, New York is gratefully acknowledged for fabricating polystyrene fibers for this experiment. This work was supported by the Laser Fusion Feasibility Project at the Laboratory for Laser Energetics which has the following sponsors: Empire State Electric Energy Research Corporation, General Electric Company, New York State Energy Research and Development Authority, Northeast Utilities Service Company, Ontario Hydro, Southern California Edison Company, The Standard Oil Company, and the University of Rochester. Such support does not imply endorsement of the content by any of the above parties.

[1] D. L. Matthews, P. L. Hagelstein, M. D. Rosen, M. J. Eckart, N. M. Ceglio, A. U. Hazi, H. Medecki, B. J. MacGowan, J. E. Trebes, B. L. Whitten, E. M. Campbell, C. W. Hatcher, A. M. Hawryluk, R. L. Kauffmann, L. D. Pleasance, G. Rambach, J. H. Scofield, G. Stone, and T. A. Weaver, Phys. Rev. Lett. **54**, 110 (1985).
[2] D. Jacoby, G. J. Pert, S. A. Ramsden, L. D. Shorrock, and G. J. Tallents, Opt. Commun. **37**, 193 (1981).
[3] J. M. Seeley, C. M. Brown, U. Feldman, M. C. Richardson, B. Yaakobi, and W. E. Behring, Opt. Commun. **54**, 289 (1985).
[4] M. C. Richardson, R. Epstein, O. Barnouin, P. A. Jaanimagi, R. Keck, H. Kim, R. S. Majorbanks, S. Noyes, J. M. Soures, and B. Yaakobi, Phys. Rev. A **33**, 1246 (1986).
[5] H. Kim, T. F. Powers, and J. F. Mason, J. Vac. Sci. Technol. A **2**, 649 (1984).
[6] D. Glocker, J. Vac. Sci. Technol. A **1**, 877 (1983).
[7] S. G. Noyes and H. Kim, J. Vac. Sci. Technol. A **3**, 1201 (1985).
[8] Polystyrene fibers were fabricated by P. Park, Mobil Chemical Co., Macedon, NY.
[9] R. W. Springer and C. D. Hosford, J. Vac. Sci. Technol. **20**, 462 (1982); R. W. Springer and D. S. Catlett, Thin Solid Films **54**, 197 (1978); R. W. Springer, B. L. Barthell, and D. Rohr, J. Vac. Sci. Technol. **17**, 437 (1980).
[10] D. G. Peiffer, T. J. Corley, G. M. Halpern, and B. A. Binker, Polymer **22**, 450 (1981).
[11] H. Kim, T. Powers, and J. Mason, J. Vac. Sci. Technol. **21**, 900 (1982).
[12] LLE Review, University of Rochester, Vol. 9, 21 (1981).

Appendix IV

LASER GENERATED X-RAY SOURCE FOR TIME-RESOLVED BIOLOGICAL AND MATERIAL STRUCTURE STUDIES

B. Yaakobi, R.D. Frankel,[1] J.M. Forsyth,[1]
and J.M. Soures

Laboratory for Laser Energetics
University of Rochester
Rochester, New York 14623

ABSTRACT

The interaction of high-intensity, focused, nanosecond laser light with matter results in the production of high temperature plasmas that emit an intense pulse of x-rays. By an appropriate choice of the target and laser parameters, one can generate an essentially continuous spectrum or a quasi-monochromatic radiation. The continuous radiation falls off in intensity above a few keV of photon energy; intense spectral lines can be produced at energies below about 8 keV. The two main unique characteristics of this x-ray source are: (a) the x-ray flux in a single pulse is sufficiently intense to record a diffraction pattern or an absorption spectrum so that time resolution on a nanosecond scale is feasible. (b) This essentially point-source enables focusing the x-ray radiation for increased flux on the sample. Our laser-generated source has been coupled to a high-numerical aperture grazing-angle x-ray camera. With this system, nanosecond x-ray diffraction patterns at resolutions of 200-4 Å, have been obtained on various biological and chemical test samples. A preliminary kinetic diffraction study has been performed on the purple membrane of the Halobacterium halobium. Structural alterations were observed one millisecond after stimulation with a visible light pulse. In another application, the continuum radiation from an

[1]Present address: Hampshire Instruments Inc., Rochester, New York.

imploding target was used to record an absorption fine-structure of sulfur in gypsum crystals.

I. SOURCE DESCRIPTION

It is well known that hot plasmas of small dimensions may be formed by focusing high-intensity laser pulses onto solid targets. Using multistage Nd^{+3}:glass lasers, constructed in connection with experiments in inertial confinement fusion, plasma electron temperatures of approximately one kilovolt (10^{7}°K) may be attained. Under appropriate conditions, efficient x-ray production of photon energy below 8 keV may be attained (1,2).

The laser used in all of our work to date is the University of Rochester's Glass Development Laser (GDL), a seven-stage, single-beam Nd^{+3}:glass laser (3) constructed as a prototype for the 24-beam OMEGA laser system (4), both at the Laboratory for Laser Energetics. This laser produces single pulses of selectable duration from 50 ps to 1 ns at a repetition rate of two shots per hour. Single-pulse energies of up to 150 J at a wavelength of 1054 nm are produced in 1 ns pulses.

The radiated spectrum may contain strong line components of several keV photon energy, if atomic constituents of the target have lines in this part of the spectrum. In flash x-ray diffraction which requires monochromatic radiation, we wish to exploit the production of line radiation to the maximum extent. In order to maximize the intensity of line radiation, we employ a transition with a high oscillator strength and create a plasma populated predominantly by the ion of interest. The dominent ionization stage should have an ionization potential of 3-5 times the plasma temperature. We find that plasmas created from elements with atomic numbers in the range 15-25, composed primarily of helium-like and hydrogen-like ions, meet these requirements. Rate equation analysis of the excitation processes in such plasmas suggest that ionization equilibrium will be achieved in a time on the order of 10^{-10} sec, significantly shorter than the laser pulses used in our experiments (5).

A series of spectra obtained under typical experimental conditions in our facility is given in Fig. 1. Laser energies on target varied between 150 and 175-J so that the focused pulse had an intensity of approximately 3×10^{15} W/cm^2. The most prominent group of lines in each spectrum includes the helium-like $1s^2\ ^1S_0$ - $1s2p\ ^1P_1$ transition (labeled w), the associated intercombination lines from the $^3P_2$ and $^3P_1$ levels (labeled x, y), and satellite lines arising from dielectronic recombination to doubly excited levels in the lithium-like ion (labeled j, k). The overall relative spectral bandwidth of this group of lines (i.e. w, x, y, j, k) is of the order of 1%

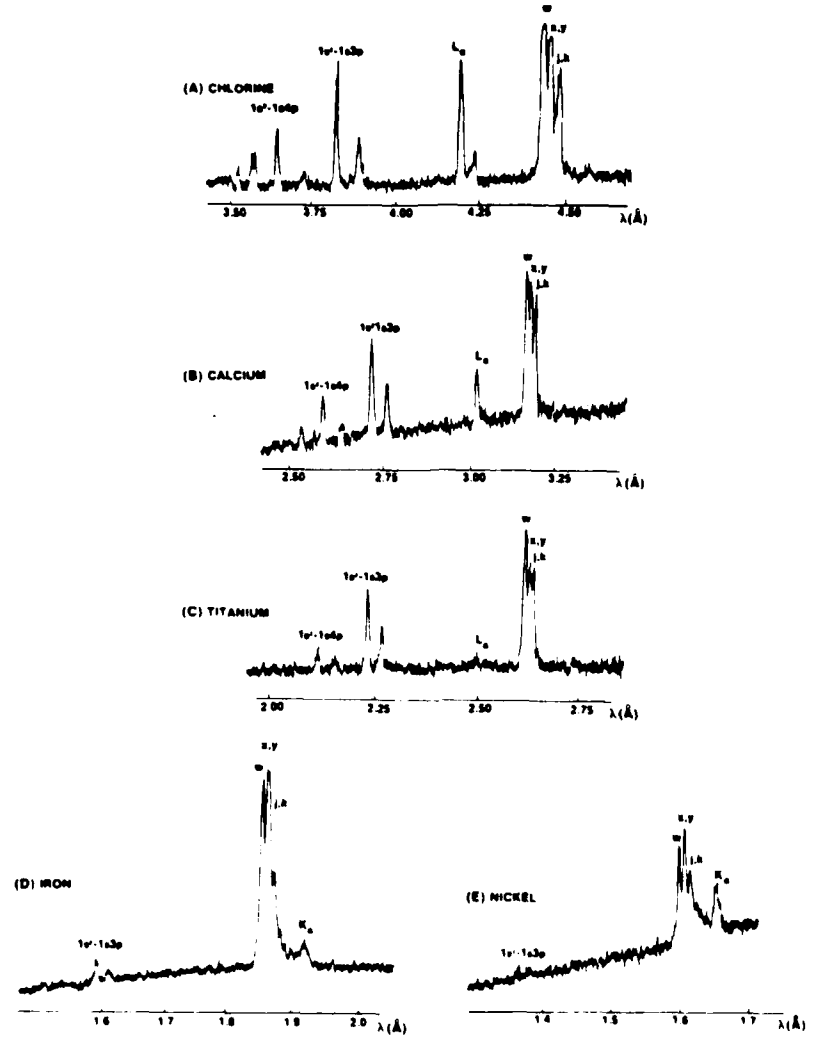

Fig. 1 X-ray line emission from 700 ps, 1054nm laser pulses focused to 100 μm on flat targets of calcium, titanium, iron and nickel.

or less so that in many applications the fine structure displayed here is unimportant. The nearest spectral component to this group is the 1s $^2S_{\frac{1}{2}}$ - 2p $^2P_{\frac{1}{2}}$ transition (labeled Lα) from the hydrogen-like ion and an associated helium-like satellite line. It will be observed that as the atomic number of the target increases the intensity of this line drops rapidly compared to the falloff in the intensity of the helium-like ion resonance radiation.

For elements heavier than phosphorous, the energy of the helium-like resonance line group lies slightly below the K-absorption edge of the solid material. Thus a thin foil of the target material may be used to remove the other line components present in the spectrum. We illustrate this by means of three chlorine plasma spectra obtained under identical conditions to those described above, except that saran foils were placed in front of the crystal spectrograph. These spectra are shown in Fig. 2. Figure 2a is essentially unfiltered (except for a 1-mil beryllium foil used in all cases to keep light out of the spectrograph). Figure 2b shows the spectrum recorded through a 0.5-mil saran foil while Fig. 2c shows the spectrum through a 1.0-mil foil. The transmission of the helium-like resonance line through the 1.0-mil saran foil is in excess of 50%.

The x ray pulse duration is about equal to that of the laser pulse. For many applications, including x-ray diffraction, the plasma is effectively a point source (6,7).

Recent advances in nonlinear optics have made possible the conversion of the infrared output from high peak power Nd^{3+}: glass lasers to the ultraviolet (third harmonic) with intrinsic efficiencies approaching 80% (8). For the past three years such a frequency conversion system has been employed on the GDL facility (3). There are many benefits to the use of short-wavelength laser radiation in target interaction experiments. Among these are a greatly enhanced degree of collisional absorption of the laser light in the target, and coupling of the laser energy into higher density regions of the plasma. In our application we observe a ten-fold increase in x-ray line emission in the spectral range of 2-5 Å with the use of ultraviolet laser pulses compared to infrared pulses of similar energy (1). All our biostructural kinetic experiments have been performed using the frequency tripled GDL facility. We next discuss in some detail the measurements of x-ray yield of individual spectral lines from a laser-irradiated target.

II. X-RAY YIELD OF SPECTRAL LINES

The application of x-rays from a laser target as a probe of transient phenomena has recently received increasing attention. X-ray radiography (back-lighting) is being developed as perhaps the most promising way for diagnosing cold, highly-compressed laser targets (9). X-rays from laser targets have also been used recently to record the diffraction pattern from a crystal protein (10) and the K-edge fine-structure absorption spectrum of sulfur in a gypsum crystal (11). Finally, x-ray pumping leading to lasing in the soft x-ray region has been under active study, employing either resonant or photo-ionization

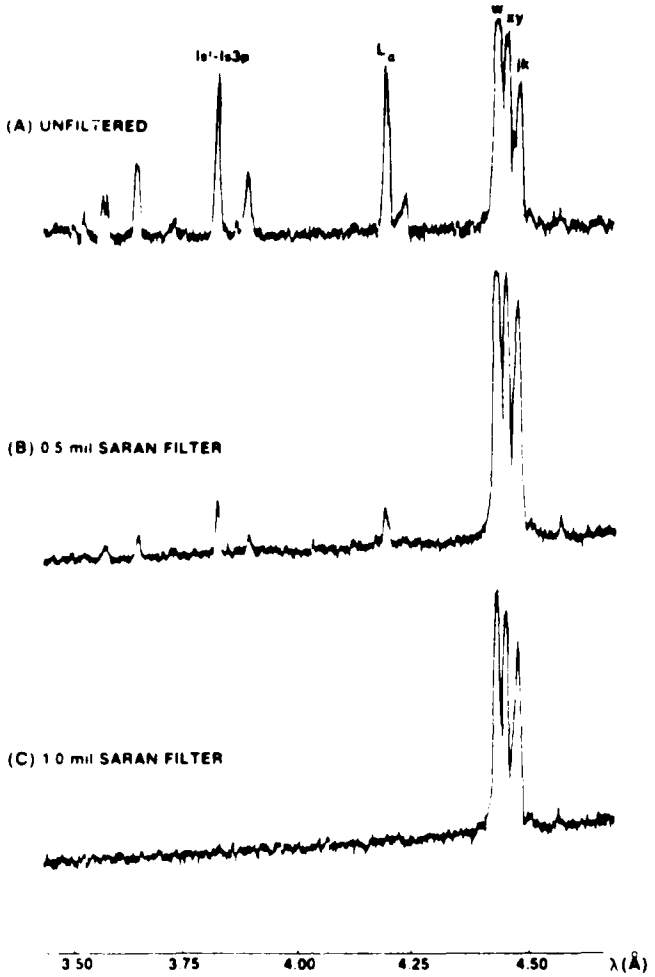

Fig. 2 Chlorine spectra from saran targets. Filtration for (A) 25 μm Be; (B) 25 μm Be + 12.5 μm saran; (C) 25 μm Be + 25 μm saran. In (C) the transmission of the resonance line and its satellites was 57%, while all other lines were almost completely absorbed. (From Ref. 32.)

type pumping (12). In some of these applications a quasi-monochromatic source is required (radiography, diffraction, resonant pumping) whereas the others require a wide-band continuum source. We find that both lines and continuum increase significantly in intensity in going from infrared to ultraviolet target irradiation.

The flat targets used in this study were glass, saran, titanium and nickel. X-ray line spectra of the helium-like and hydrogen-like ionization states of the elements Si, Cl, Ti and Ni were recorded. Gypsum, P.E.T., germanium and LiF crystals were used alternatively to record the respective spectra.

Fig. 3 shows as an example the spectrum obtained from a titanium target irradiated with a 40 J, 500 ps pulse focused with a f/12 lens to give an irradiance of about $5 \times 10^{14} W/cm^2$.

Short laser pulses (100 ps, 0.2 TW) produced nearly the same x-ray conversion efficiency as longer pulses for Si through Ni. Defocusing the laser to lower the irradiance by more than an order of magnitude typically increased the conversion efficiency by a factor <1.5. All this indicates that x-ray yield scales primarily with total laser pulse energy, at least within the present parameter range.

Fig. 4 compares these results with x-ray yield data obtained from the same laser operating at a wavelength of 1.054 μm. Its output energy was boosted by four active mirrors (novel type laser amplifiers (13)) to produce 700 ps pulses of 175 J energy. An f/4 focusing lens produced an irradiance of 10^{15} W/cm^2. As seen in Fig. 4, UV irradiation is more efficient in producing x-rays, by a factor of about 10, which decreases with increasing Z. This observation at high Z is believed to be due to the significant presence of fast electrons in IR laser irradiation which can contribute to the excitation of high energy x-ray lines.

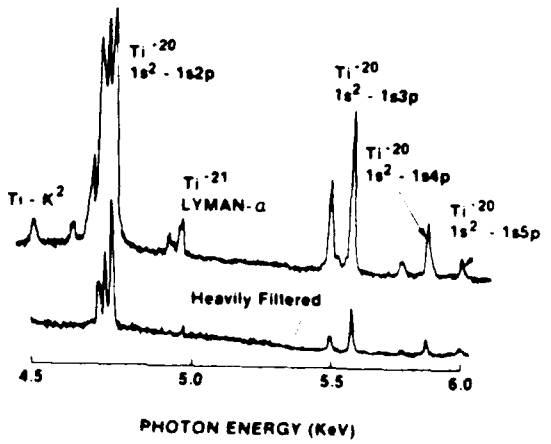

Fig. 3. X-ray spectrum emitted from titanium target irradiated by a 0.35 μm laser. Lower trace shows the simultaneously obtained spectrum through a 15 μm thick aluminum foil. (From Ref. 1.)

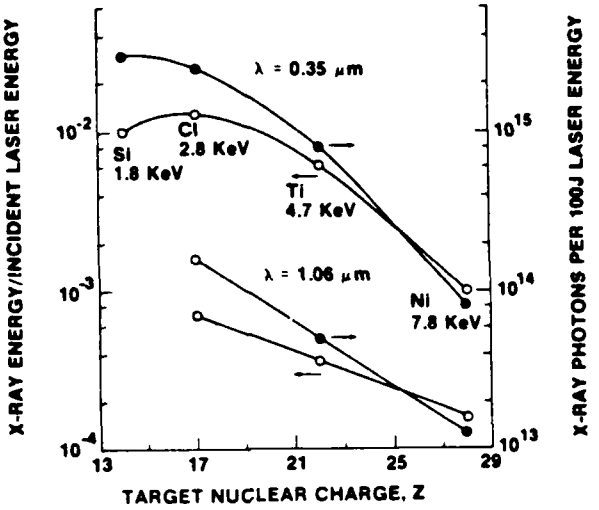

Fig. 4 Quasi-monochromatic X-ray conversion efficiency versus the nuclear charge Z of the emitting ion. X-ray emission into 4π refers to the resonance line $1s^2$ -1s2p of the helium-like ionization state. Upper curves 40 J, 500 ps, lower curves, 175 J, 800 ps. (From Ref. 1).

III. SMALL-ANGLE DIFFRACTION STUDIES

A. X-ray Optics

Since the x-ray emission from these targets is roughly isotropic, the design of high intensity x-ray beamline facility presents a challenge in maximizing the collection and transport of x-rays. Furthermore, in an application such as low angle diffraction, the residual divergence of the beam limits the angular resolution of the system. This constrains the x-ray collection system to be a focusing system. The point nature of the laser-driven source, combined with its highly reproducable position in space, is very important because it permits use of a simple, high efficiency, grazing angle focusing system.

Our camera is shown schematically in Fig. 5. We use a toroidal mirror in the form of a truncated ellipsoid to focus the x-rays. Toroidal x-ray collectors pioneered by Henke (14) and Elliot (15) have collection efficiencies up to a factor of 100 times those of traditional, Franks, bent mirror optics. Our mirror was fabricated from a CERVIT substrate in the optical shop at the University of Rochester and coated with nickel in the LLE target fabrication facility. In this geometry, it can be shown that the maximum useful collection solid angle is

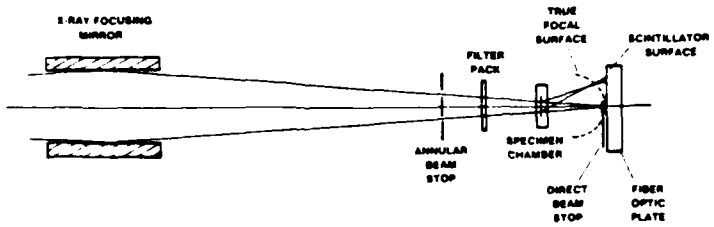

Fig. 5 Schematic diagram of X-ray diffraction camera. The true focal surface of the camera is a sphere tangent to the sample and also tangent to the flat phosphor plane. (From Ref. 32.)

of the order of θ_c^2, where θ_c is the critical angle for total reflection of x-rays (14). Nickel is a good x-ray reflector in the 2-5Å range and results in a collection solid angle for our system of approximately 2×10^{-4}sr. An isolated space of approximately 20 cm in front of the x-ray detector and camera focus is available to position specimens.

B. Detection and Data Analysis

A schematic diagram of our detection system is shown in Fig. 6. In experimental shots up to 10^{10} photons of foil-filtered x-rays at 4.45 Å were delivered to specimens on each GDL laser shot. Because of the unprecendented rate of delivery of x-rays in this system it is impossible to use counter tubes as detectors. Solid state detectors have many desirable characteristics, but are not yet available in sufficiently large area arrays to be suitable for our application, while film is not sensitive enough to record good patterns with presently available fluxes. On the other hand, TV detectors have no soft x-ray response because of the windows used. This latter problem may be overcome by using a thin scintillator material to convert the x-rays to visible light (16).

The true focal surface of the camera is a sphere tangent to the focal point of the camera and to the vertex of the specimen (14). Therefore, our early experiments with flat scintillator plates limited our observation to low scattering angles due to limited focal depth. Our goal was to achieve satisfactory focus at up to 35° scattering angles over a 40-mm-diameter detection field, which requires a specimen position as close as 3.5 cm from focus. We estimated that a section of a spherical

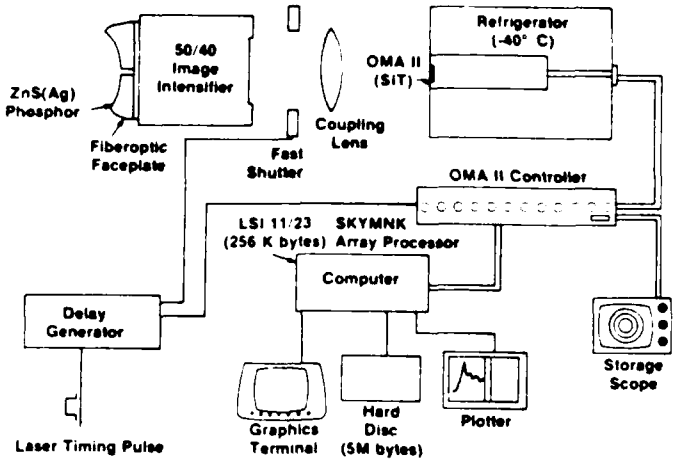

Fig. 6 X-ray detection system. (From Ref. 33.)

focal surface 5 cm in diameter would permit such a close working distance to be achieved with acceptable sharpness. Satisfactory deposition of a thin ZnS:Ag scintillator onto a glass surface of this curvature was achieved by Thomas Electronics, Inc. when the plates were supplied with a 3.2-mm hole drilled at the vertex. This hole also served the zero-order (direct) beam stop.

The output of the scintillator is fiberoptically coupled to a VARO 50/40 mm microchannelplate (MCP) image intensifier set to a gain of 30,000. For low-angle experiments, a flat phosphor-coated face plate can be used, because the sample-phosphor distances are large (> 10 cm), providing a flatter focal sphere. Our readout format includes 224 lines of 448 channels per line. Channel dwell time is typically 140 usec; thus an entire scan requires 14 seconds. The 1216 controller is interfaced to an LSI 11/23 (Digital Equipment Corporation (DEC) via a DRV-11 parallel interface card. The 11/23 has been modified to accommodate 1 megabyte of main memory addressed through memory management. All programming is performed in the computer language Forth (19,20).

C. Experimental Results

We now present some x-ray diffraction patterns from biological specimens to illustrate the performance capabilities of the facility. Biological specimens present especially chal-

lenging tests because of their relatively low x-ray scattering power. The operation of the facility for kinetic experiments will be described; however, detailed results on photostimulated membrane systems will be presented elsewhere (21). The results were all obtained using foil-filter soft x-ray radiation at 4.45 Å produced from laser irradiated saran targets. This wavelength was chosen to enable very thin specimens to be used while maintaining good x-ray scattering efficiency. Our interest in thin specimens derived from our desire to perform photostimulation on optically dense specimens.

A photobiological system of widespread interest in recent years is the purple membrane (PM) of the Halobacterium halobium. This membrane is composed of an almost perfect, hexagonally packed, two-dimensional array of one protein, bacteriorhodopsin (BR) (22). Like mammalian rhodopsin, BR contains the chromophore retinal and has a photocyle with a time course and spectral characteristics similar to rhodopsin (23). It has been shown that BR functions as a light-driven proton pump which sets up a transmembrane hydrogen ion gradient (24). It is of interest to determine if molecular conformational changes are associated with the ion pumping function. The PM serves not only as a demonstration system for low-angle x-ray diffraction, but may be used to demonstrate some of the techniques which must be employed in kinetic experiments.

Figure 7 shows a powder diffraction pattern from a dried pellet of purple membrane recorded by using a single nanosecond duration laser pulse of 45 J at 351 nm. The diffraction pattern consisted of a set of bright circular rings on the scintillator detector, a sector of which was circularly average by the 11/23 computer to produce this display. The specimen consisted of an array of membrane fragments or platelets, whose planes were partially oriented by drying onto a (1-2 μm) polypropylene support. The highest order reflection shown corresponds to 7-Å resolution in the plane of the membrane (and is the highest order reflection to be reliably phased by any group to date). The reflectons are all indexed on a hexagonally packed lattice after Blaurock and Stoeckenius (22). This pattern was partially corrected for system geometrical distortions as well as for non-uniform sensitivity of the detection system. Compared to published diffraction patterns, (25,26), we have achieved about a factor of 2-3 lower instrumental resolution and somewhat reduced signal to noise ratio. However, all of the main orders of diffraction are present at the appropriate intensity ratios and positions.

A thin specimen chamber was constructed which permits a supply of gas to flow across the specimen and which has an entrance window transport to both light and x-rays. When using 4.45 Å radiation a saran window may be used.

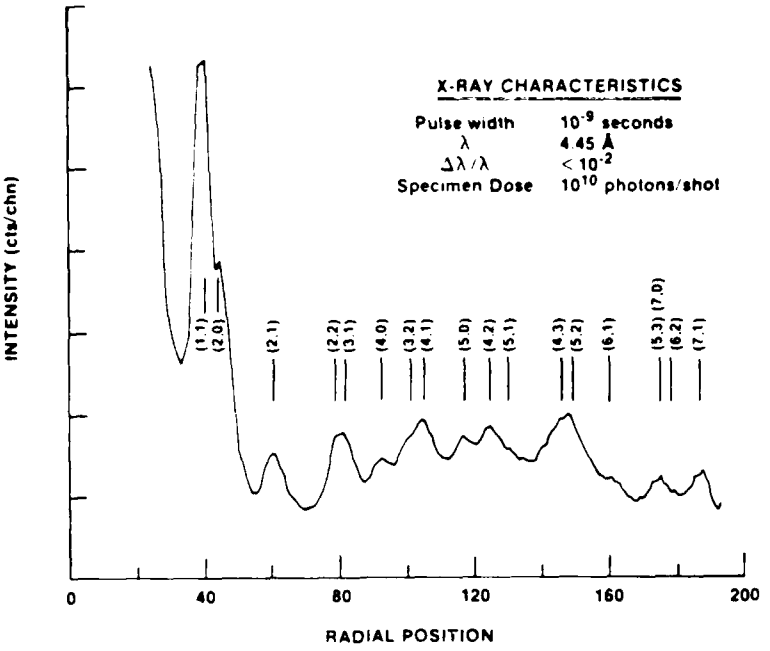

Fig. 7 Circular average of a dried purple membrane (PM) powder pattern. Background scattering was not removed. This sample displayed background scattering caused by cracking on drying. The abscissa is in units of T.V. channels. (From Ref. 33.)

In the design of a kinetic x-ray diffraction experiment, it must be kept in mind that diffraction is a technique which probes the average structure of bulk material. If a structural perturbation is to be introduced, care must be taken to uniformly perturb as high a fraction of the specimen as possible to minimize the ambiguity inherent in interpreting data acquired from a mixed phase system. Purple membrane is typical of many photoactivated systems which might be studied in that it exhibits a finite quantum efficiency for photoactivation, in this case, 30% (27,28). Because we were interested in study of structural activity during the formation of a stable photointermediate state of the system, we decided to employ a train of light pulses (frequency-doubled Nd^{+3}:YAG laser) to successively raise an increasing fraction of the system to the photoactive state. This strategy was dictated by the fact that prior to the formation of a stable photointermediate the pre-

sence of light maintains an equilibrium between the ground state and photocycling populations.

Figure 8 displays a background-corrected diffraction pattern obtained 1 msec after stimulation of a light adapted, dried, membrane stack. The broad rising and falling background in the 0.05-0.11 Å^{-1} region of the diffraction pattern, is indicative of scattering from BR monomers or trimers (29), and is suggestive of significant disorder in the specimen after stimulation.

For several reasons we believe the disorder observed is not lattice disorder caused by heating due to photostimulaton. First, stimulation of dried, dark adapted membranes showed no appreciable effect on diffraction patterns. Second, calculations indicate that the stimulus-induced temperature rise in the sample should be less than 5°C. Moreover, the pulse train stimulus scenario limits impulse heating. We suggest substitution (or unit cell) disorder is the predominent alteration causing the disordered scattering evident in Fig. 8. Trimeric structures may be partially disordered and still yield a .03 Å^{-1} peak, or the trimers may move as a unit upon BR activation. We have not observed a pure trimer or pure monomer pattern with the absence of lattice structure.

The lattice constant in purple membrane is approximately 63 Å and much of the structural activity is observed at substantially smaller scale length. In other membrane systems and in

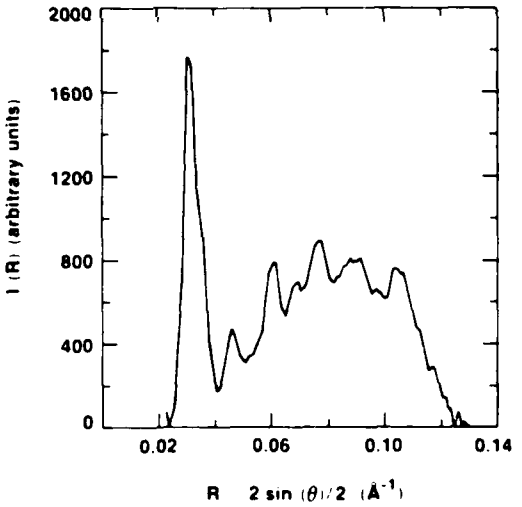

Fig. 8 Circular average of dried PM x-ray diffraction pattern, one millisecond after stimulation, fully corrected for geometric distortion; the monotonically decreasing background was subtracted from the raw data.

many polymer studies, however, much longer scale lengths are of interest. Thus the low-angle performance of the camera system is important. In Fig. 9, we present a portion of a digital image showing the first order lamellar diffraction from a dipalmitoyl lecithin multilayer structure with a basic repeat period of 55 Å (30). This specimen was placed approximately 20 cm from the focus of the camera, and foil filtered x-ray radiation at 4.45 Å was used. The specimen was oriented in a low-angle, reflection geometry and intercepted only a small portion of the annular, x-ray beam. The natural mosaic structure of the multilayer is evident in the pronounced, arc-like scattering around the (saturated) central reflection peak. The large space between this peak and the zero order suggested that a much lower angle reflection could be observed. These results suggest many possible studies of dynamic structural phenomena in materials with large repeat distances. Other time-resolved studies, such as contracting muscle, or solution scattering from proteins, may require thicker samples, dictating use of more energetic x-rays.

Recently we have acquired a nanosecond diffraction pattern from a 200 μm thick polyethylene film with helium-like Ti radiation at 2.6 Å. This pattern displayed a reflection at 4 Å (31). This opens up the possibility of high angle kinetic x-ray diffraction studies.

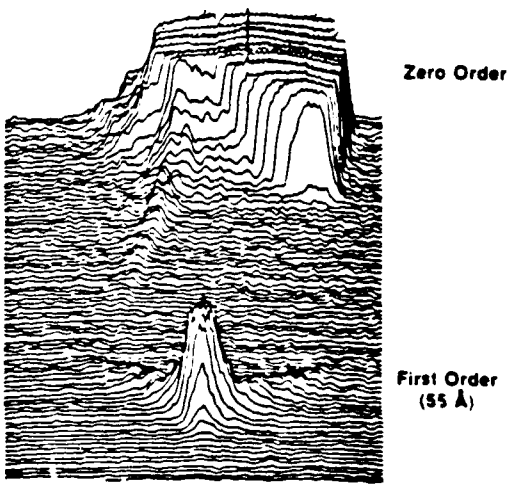

Fig. 9 Single shot x-ray diffraction pattern from dipalmitoyl lecithin multilayer in helium atmosphere. The specimen was placed at a glancing angle thus intercepting only 10-20% of the full annullar x-ray beam.

IV. X-RAY-ABSORPTION FINE-STRUCTURE MEASUREMENT USING A LASER-COMPRESSED TARGET AS A SOURCE

Recently, x-ray continuum radiation from a laser-produced plasma source has been used (34) to record an EXAFS spectrum of aluminum (EXAFS (35) stands for extended x-ray-absorption fine structure and requires a source of continuum radiation). The flat target in that experiment was irradiated by a single laser beam of pulse duration 3.5 nsec. We show here that when a spherical target is symmetrically imploded by a multibeam laser system the resulting x-ray source is better suited for such experiments: for the same laser energy and for targets of comparable atomic composition the continuum radiation from an imploded target is more intense by at least an order of magnitude. The x-ray emitting plasma in both cases has a temperature of 10^6-10^7K; however, whereas the expanding plasma near a flat target has an electron density of order 10^{21} cm^{-3}, the density at the center of a converging spherical target is of order 10^{23} cm^{-3}.

The fine structure is measured in diffraction rather than in transmission, enabling the observation of the anomalous scattering near the K edge (36); also, the fine structure closer to the K edge (XAFS) is measured rather than the extended fine structure. EXAFS (35), anomalous scattering (36), and XAFS (37) are useful in determining the structure of

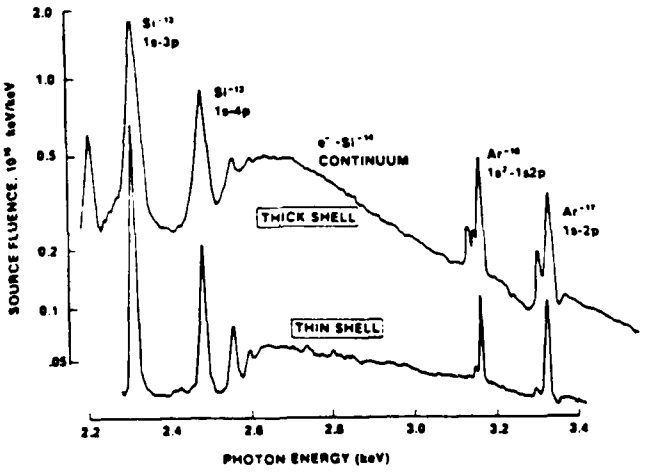

Fig. 10 Part of the x-ray spectrum from a thick-shell (high compression) and thin-shell (low commpression) target implosions. (From Ref. 11.)

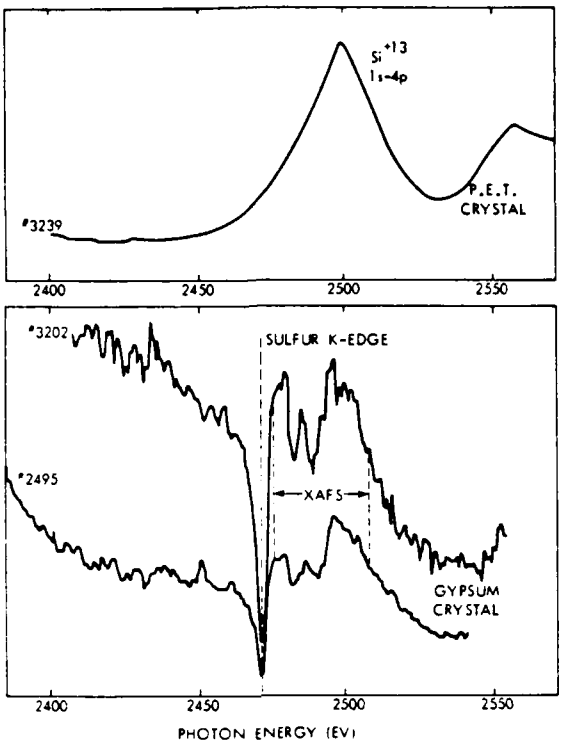

Fig. 11 Three target experiments. On shots No. 3202 and 2495 a gypsum crystal was used and showed fine structure near the K edge of sulfur, whereas the PET crystal used on shot No. 3239 showed the spectrum without sulfur absorption. (From Ref. 11.)

chemical or biological samples, and as noted in Ref. 34, the short laser pulse enables the application of these methods to transient or dynamic phenomena.

The data shown here were obtained with the ZETA six-beam Nd:glass laser system (38) at the National Laser Users Facility of the University of Rochester. Fifty-psec laser pulses of peak power 2 TW were used to implode glass shells of diameter 50-60 μm and wall thickness 1-3 μm, filled with argon of pressure 7-14 atm. The combination of relatively thick shells and radiational cooling by the argon produced a high denisty in the fill gas and in the imploding part of the glass shell (39). This resulted in a high-intensity x-ray continuum emitted from a 30-μm-size region in the center of the target. Figure 10 compares part of the spectra for two shots and shows that a higher target compression (achieved with the thicker shell) leads to enhanced emission of continuum radiation.

The observation of XAFS using an imploded microballoon is illustrated in Fig. 11 where a smaller section of the spectra of three target experiments are shown. For the two lower spectra a gypsum crystal was used and anomalous scattering features due to sulfur atoms in the crystal are cleary seen. Two target shots are shown in order to demonstrate the repeatability of the results. The corresponding spectrum measured with a pentaerythritol (PET) crystal shows the incident, unscattered spectrum. All the features normally measured in absorption appear in diffraction as well, since the diffracted intensity is proportional to the square of the atomic structure factor, which entails the absorption coefficient (40).

ACKNOWLEDGEMENTS

This work was supported by the U.S. Department of Energy Office of Inertial Fusion under contract DE-AC08-80DP40124 and by the Laser Fusion Feasibility Project at the Laboratory for Laser Energetics which has the following sponsors: Empire State Electric Energy Research Corporation, General Electric Company, New York State Energy Research and Development Authority, Northeast Utilities Service Company, Southern California Edison Company, The Standard Oil Company (Ohio), the University of Rochester. Such support does not imply endorsement of the content by any of the above parties.

REFERENCES

1. Yaakobi, B., Bourke, P., Conturie, Y., Delettrez, J., Forsyth, J. M., Frankel, R. D., Goldman, L. M., McCrory, R. L., Seka, W., and Soures, J. M. (1981). Optics Comm. 38, 196.
2. Mead, W. C., et al. (1983). Phys. Fluids 26, 2316.
3. Seka, W., Soures, J. M., Jacobs, S. D., Lund, L. D., and Craxton, R. S. (1981). IEEE J. Quant. Electron. QE-17, 1689.
4. Bunkenburg, J., et al. (1981). IEEE J. Quant. Electron. QE-17, 1620.
5. Whitney, K. G., and Davis, J. (1974). J. Appl. Phys. 45, 5294 .
6. Shay, H. D., Haas, R. A., Kruer, W. L., Boyle, M. J., Phillion, D. W., Rupert, V. C., Kornblum, H. N., Rainer, F., Slivinsky, V. W., Koppel, L. N., Richards, L., and Tirsell, K. G. (1978). Phys. Fluids 21, 1634.
7. Jackel, S., Perry, B., and Lubin, M. (1976). Phys. Rev. Lett. 37, 95.

8. Seka, W., Jacobs, S. D., Rizzo, J.E., Boni, R., and Craxton, R. S. (1980). Optics Comm. 34, 469.
9. Key, M. M., Lewis, C. L. S., Lunney, J. G., Moore, A., Hall, T. A., and Evans, R. G. (1978). Phys. Rev. Lett. 41, 1467.
10. Frankel, R. D., and Forsyth, J. M. (1979). Science 204, 622.
11. Yaakobi, B., Deckman, H., Bourke, P., Letzring, S., and Soures, J. M. (1980). App. Phys. Lett. 37,767
12. Bunkin, F. V., Derzhiev, V. I., and Yakovlenko, S. I. (1981). Sov. J. Quant. Electron. 11, 971.
13. Abate, J. A., Lund, L. D., Brown, D. C., Jacobs, S. D., Refermat, S., Kelly, J. M., Gavin, M., Waldbillig, J., and Lewis, D. (1981). App. Optics 20, 351.
14. Henke, B. L. and DuMond, J. W. M. (1955). J. Appl. Phys. 26, 903
15. Elliott, A. (1965). J. Sci. Instrum. 42, 312 .
16. Reynolds, G. T., Milch, J. R., and Gruner, S. M., (1977). IEEE Trans. Nucl. Sci. NS-24, 501.
17. Staerk, H., Mitzkus, R., and Meyer, H. (1981). Appl. Optics 20, 471.
18. Liesegang, G. W. and Smith, P. D. (1981). Appl. Optics 20, 2604.
19. Moore, C. (1974). J. Astron. and Astrophys., Suppl. 15, 497.
20. Kogge, P. M. (1982). IEEE Computer 15, 22.
21. Frankel, R. D. and Forsyth, J. M., to be published.
22. Blaurock, A. E. and Stoeckenius, W. (1971). Nature New Biol. 233, 153.
23. Ottolenghi, M. (1982). "Methods in Enzymology," Ed. L. Packer, Vol. 88 (New York, Academic Press, p. 470.
24. Oesterhelt, D. and Stoeckenius, W. (1973). Proc. Natl. Acad. Sci. U.S.A. 20, 2835.
25. Henderson, R. J. (1975). Mol. Biol. 93, 123.
26. Blaurock, A. E. (1975). J. Mol. Biol. 93, 1039.
27. Goldschmidt, C. R., Kalisky, O., Rosenfeld, T. and Ottolenghi, T. M. (1977). Biophys. J. 17, 179.
28. Kalisky, O., Goldschmidt, C. R., and Ottolenghi, M. (1977). Biophys. J. 19, 185.
29. Kataoka, M. and Ueki, T. (1980). Acta. Cryst. A36, 282.
30. Blasie, J. K., Forsyth, J., Frankel, R. D., Herbette, L., and Pascolini, D. (Unpublished).
31. Frankel, R. D., and Kim, H. (Unpublished).
32. Frankel, R. D. and Forsyth, J. M. (1982). Methods of Enzymology Ed. L. Packer, Acad. Press 88, 276.
33. Frankel, R. D. and Forsyth, J. M. To be published in Review Sci. Instr.
34. Mallozzi, P.J., Schwerzel, R.E., Epstein, H.M., and Campbell, B.E. (1979), Science 206, 353.

35. See, for exammple, Lytle, F.W., Sayers, D.E., and Stern, E.A. (1975). Phys. Rev. B 11, 4825.
36. See, for example, Phillips, J.C., Wlodawer, A., Goodfellow, J.M., Watenpaugh, K.D., Sieker, L.C., Jensen, L.H. and Hodgson, K.O. (1977). Acta Crystallogr. A 33, 445.
37. See, for example, Shulman, R.G., Yafet, Y., Eisenberger, P., and Blumberg, W.E. (1976). Proc. Natl. Acad. Sci. USA 73, 1384.
38. Bunkenberg, J. and Seka, W. (1979). In Proceedings of the IEEE Conference on Laser Engineering and Applications, New York, Digest of Technical Papers (unpublished), p. 96.
39. Yaakobi, B., Skupsky, S., McCrory, R.L., Hooper, C.F., Deckman, H., Bourke, P., and Soures, J.M. (1980). Phys. Rev. Lett. 44, 1072.
40. Bienenstock, A. (1977). In The Structure of Non-Crystalline Materials, ed. Gaskell, P.H. (Taylor and Francis, London), p. 5.

END

3-87

DTIC